# PromptMoG: Enhancing Diversity in Long-Prompt Image Generation via Prompt Embedding Mixture-of-Gaussian Sampling

Bo-Kai Ruan Teng-Fang Hsiao Ling Lo Yi-Lun Wu Hong-Han Shuai National Yang Ming Chiao Tung University

{bkruan.ee11,tfhsiao.ee13,linglo.ee08,yilun.ee08,hhshuai}@nycu.edu.tw

## **Abstract**

Recent advances in text-to-image (T2I) generation have achieved remarkable visual outcomes through large-scale rectified flow models. However, how these models behave under long prompts remains underexplored. Long prompts encode rich content, spatial, and stylistic information that enhances fidelity but often suppresses diversity, leading to repetitive and less creative outputs. In this work, we systematically study this fidelity-diversity dilemma and reveal that state-of-the-art models exhibit a clear drop in diversity as prompt length increases. To enable consistent evaluation, we introduce LPD-Bench, a benchmark designed for assessing both fidelity and diversity in long-prompt generation. Building on our analysis, we develop a theoretical framework that increases sampling entropy through prompt reformulation and propose a training-free method, PromptMoG, which samples prompt embeddings from a Mixture-of-Gaussians in the embedding space to enhance diversity while preserving semantics. Extensive experiments on four state-of-the-art models, SD3.5-Large, Flux.1-Krea-Dev, CogView4, and Qwen-Image, demonstrate that PromptMoG consistently improves long-prompt generation diversity without semantic drifting.

# 1. Introduction

Text-to-image diffusion has become a practical engine for content creation across design ideation, advertising, media asset production, education, and interactive prototyping [18, 24, 26]. For these use cases, two properties are essential: fidelity to the prompt and diversity under the same prompt, *i.e.*, the ability to produce multiple distinct yet semantically valid images that all satisfy the text. Diversity enables creative exploration, supports downstream selection and editing, improves fairness by avoiding a single stereotypical rendering, and strengthens data augmentation for training pipelines. Compared with GANs [3, 9, 36], diffusion models are markedly better at covering modes and are less prone to collapse since learning proceeds through a

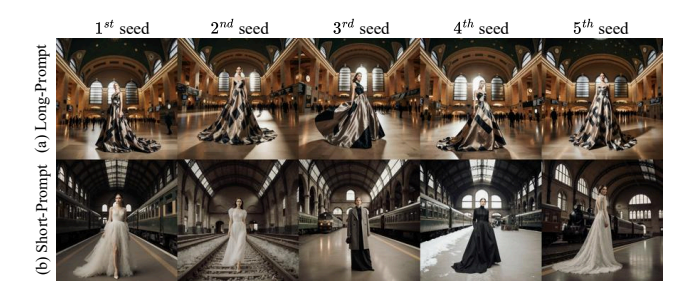


Figure 1. Qualitative comparison of diversity generated with Flux.1-Krea-Dev. Images are generated from different random seeds using (a) long prompts and (b) short prompts.

likelihood-aligned denoising objective that distributes probability mass over many valid explanations of the prompt rather than concentrating on one.

Despite these strengths, long and detailed prompts remain challenging for diversity. Specifically, long prompts typically encode detailed spatial layouts, viewpoint specifications, stylistic cues, and compositional constraints that jointly define the visual outcome. These conditions enhance semantic fidelity and allow precise alignment with user intent, but they simultaneously restrict the feasible solution space. As a result, long-prompt generation faces a dilemma between fidelity and diversity, where the model overemphasizes dominant semantic elements and suppresses alternative interpretations. Consider a portrait scene, where the long prompt further specifies the setting with soft daylight, enormous clocks on the walls, and a model wearing a silkshimmering gown with a sweeping skirt, as shown in Figure 1. Across random seeds, the generations produced under this long prompt converge to nearly identical architectural arrangements and gown designs. Even elements that are not explicitly constrained by the prompt, such as background or hair styles, fail to exhibit meaningful variation.

Enhancing diversity is important not only for artistic expressiveness but also for controllability [37, 42], because a richer set of valid samples increases the chance of satisfying complex user constraints without semantic drift. Approaches to improve diversity fall into two groups: training-

based and sampling-based. Training-based methods have mostly targeted short prompts [8, 19] and often operate on small models or require additional optimization, which limits scalability to contemporary systems. In contrast, sampling-based approaches avoid retraining [7, 20, 27], yet on long prompts, they tend to relax conditioning or overoptimize surrogate objectives, which induces semantic drift. To the best of our knowledge, no prior work explicitly addresses the diversity degradation caused by long prompts while remaining training-free to large-scale T2I models.

In this paper, we study the diversity issue under long prompts and present a plug-and-play, training-free solution that increases diversity without sacrificing semantic fidelity. Specifically, we develop a theoretical formulation that improves sampling diversity by increasing entropy in the prompt embedding space. Guided by this principle, we propose a training-free method, PromptMoG, which reformulates prompt embeddings into uniformly distributed points on a high-dimensional sphere with a constrained radius to control semantic deviation. These points are modeled as centers of Gaussian components to construct a Mixture-of-Gaussians (MoG). Conceptually, this process expands the set of available prompt variants for generation. By sampling from the constructed MoG, PromptMoG generates diverse yet semantically consistent prompts, effectively enhancing long-prompt generation diversity.

Moreover, since long-prompt diversity has not been systematically evaluated, we first build the Long-Prompt Diversity Benchmark (LPD-Bench). LPD-Bench refers to the photography taxonomy in Adobe Lightroom [1] to obtain 25 representative scene categories and generate 1000 prompts of 250-450 words that jointly specify semantic content, spatial layout, and stylistic cues, allowing analysis across varied visual themes. To better evaluate the quality of long-prompt generation, we introduce a chunkbased evaluation protocol that enforces alignment between generated content and key segments of the prompt, enabling faithful assessment of long-prompt generation. In addition to standard fidelity metrics, LPD-Bench also incorporates the Vendi Score [11] to evaluate generation diversity. Extensive experiments across several state-of-theart T2I models, including SD3.5-Large [10], Flux.1-Krea-Dev [15], CogView4 [41], and Owen-Image [35], demonstrate that PromptMoG consistently enhances diversity and outperforms heuristic baselines such as prompt chunking and existing sampling-based approaches [20, 27]. The key contributions can be summarized as follows.

- We provide the first systematic analysis of the diversity under long prompts and release LPD-Bench for faithful evaluation. Across state-of-the-art large-scale rectified flow models, LPD-Bench reveals a consistent drop in setlevel diversity as prompt length increases.
- We present a theoretical framework that connects prompt

- reformulation to increased sampling entropy and propose a training-free, plug-and-play method, PromptMoG, which samples prompt embeddings to enhance diversity.
- Experiments on the LPD-Bench show that the proposed PromptMoG outperforms four large-scale T2I models in terms of diversity while maintaining semantic fidelity.

## 2. Related Work

# 2.1. Text-to-Image Generation

Recent advances in text-to-image (T2I) generation are largely driven by the success of latent diffusion models [25, 26], which learn to progressively denoise latent representations conditioned on textual descriptions. Diffusion transformers [18, 24] improve scalability through transformer architectures, where model capacity strongly correlates with visual quality. Rectified Flow models further reformulate the diffusion process into a deterministic and efficient formulation that accelerates inference while maintaining generation quality. Beyond visual quality, recent studies have advanced the semantic fidelity of the generated results. MM-DiT [10] enhances cross-modal integration in RF-based transformers by directly concatenating both image and text tokens for attention blocks, enabling bidirectional information flow that improves text comprehension. Additionally, large language models are increasingly utilized as text encoders [4, 35, 41] to enhance prompt understanding, thereby strengthening the alignment between textual intention and visual realization. While long and compositionally rich prompts provide more detailed semantic cues and are expected to enhance fidelity, their behavior in modern T2I systems remains relatively underexplored. Existing studies on long-prompt generation [34] primarily focus on evaluating alignment and quality, with little attention to how these complex prompts influence generation diversity.

# 2.2. Diversity Enhancement for T2I generation

Generation diversity refers to the range of distinct outputs a model can produce from a given prompt. Assessing diversity measures how well a model can produce a wide range of plausible results without collapsing into repetitive or biased patterns. Early evaluations of diversity quantify the distributional overlap between generated and real samples [2, 12, 21, 28], but they depend heavily on the reference datasets. Vendi Score [11] addresses the above limitation through an unsupervised formulation based on the eigenvalue spectrum of the sample-similarity matrix, enabling diversity assessment without real data. Efforts to enhance diffusion diversity generally fall into two categories: trainingbased and sampling-based. Training-based methods modify objectives or architectures to encourage variability during learning. For example, DIG [19] employs reinforcement learning with mutual information as a reward to encourage diverse outputs, while DiADM [8] introduces a retrievalbased diversity-aware module that leverages reference images to promote variation. Although effective, these methods are dataset-specific, computationally intensive, and require retraining, which limits their scalability to large models. Sampling-based approaches improve diversity by manipulating the inference process. CADS [27] perturb conditioning signals to induce variability, whereas joint-sampling techniques [7, 20] optimize latent representations during inference to diversify generated samples. While computationally efficient, these approaches often suffer from illconstrained or over-optimized objectives, leading to semantic drift under long prompts. Overall, existing techniques target short-prompt generation and overlook the fidelity-diversity challenges unique to long-prompt settings, leaving the problem largely underexplored.

# 3. Methods

We propose PromptMoG, a training-free method designed to enhance generative diversity in long-prompt T2I models without compromising semantic fidelity. We begin with preliminaries on Rectified Flow (RF) models, which serve the primary backbone for our method. Next, we analyze the diversity degradation that arises with increasing prompt length, showing how long prompts lead RF samplers toward similar generative results. Building on these observations, we develop a theoretical formulation that supports diverse sampling by enhancing prompt embeddings from an entropy-based perspective. Finally, we introduce our PromptMoG and discuss the key design that enables effective diversity enhancement.

# 3.1. Preliminary

**Rectified Flow.** An RF-based model [17] aims to learn a *linear* probability path between the clean data distribution  $\mathbf{x}_0 \sim p_{\text{real}}$  and the standard Gaussian noise distribution  $\mathbf{x}_{t_{\text{max}}} \sim \mathcal{N}(\mathbf{0}, \mathbf{I})$ :

$$\mathbf{x}_{t_k} = (1 - t_k)\mathbf{x}_0 + t_k\mathbf{x}_{t_{\text{max}}}, \quad \forall \, t_k \in [0, t_{\text{max}}],$$

by predicting the velocity field  $\mathbf{v}_{\theta}(\mathbf{x}_{t_k}, t_k)$  defined as:

$$d\mathbf{x}_{t_k} = \mathbf{v}_{\theta}(\mathbf{x}_{t_k}, t_k) dt_k, \quad \forall t_k \in [0, t_{\text{max}}]. \tag{1}$$

Since the velocity of a linear path is constant, it can be expressed as the difference between the clean and noisy samples. Thus, the training objective for  $\mathbf{v}_{\theta}$  is formulated as:

$$\mathcal{L} = \mathbb{E}_{t_k \in [0,t_{\max}], \mathbf{x}_{t_{\max}} \sim \mathcal{N}(\mathbf{0}, \mathbf{I})} \left[ \| (\mathbf{x}_0 - \mathbf{x}_{t_{\max}}) - \mathbf{v}_{\theta}(\mathbf{x}_{t_k}, t_k) \|_2^2 \right].$$

**Sampling.** Once the velocity model  $\mathbf{v}_{\theta}$  is trained, sampling is performed by starting from the noise distribution and obtaining the Euler ODE from Equation (1) into:

$$\mathbf{x}_{t_{k-1}} = \mathbf{x}_{t_k} + (t_{k-1} - t_k)\mathbf{v}_{\theta}(\mathbf{x}_{t_k}, t_k), \tag{2}$$
 where  $\mathbf{x}_{t_{\text{max}}} \sim \mathcal{N}(\mathbf{0}, \mathbf{I}).$ 

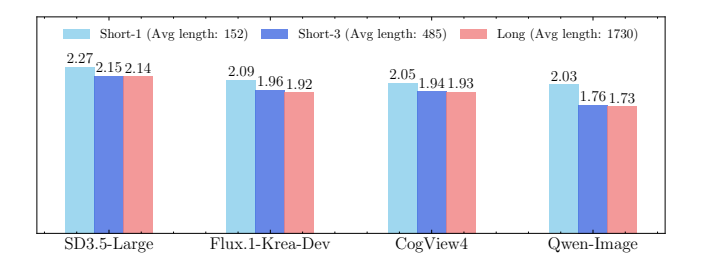


Figure 2. Comparison of diversity across different prompt lengths using the Vendi Score with InceptionV3. From left to right: using the first sentence, the first three sentences, and all sentences from each long prompt.

# 3.2. Diversity Degradation under Long Prompts

To investigate the diversity degradation caused by long prompts, we conduct an experiment using 6 different random seeds and measure the diversity of generated samples with the Vendi Score introduced in Section 4.2. We compare the Vendi Score obtained from long prompts in our LPD-Bench<sup>1</sup> with those derived from shorter variants constructed by taking only the first sentence and the first three sentences of each long prompt. As shown in Figure 2, longer prompts consistently yield lower scores across all evaluated models, indicating that diversity decreases as prompt length increases. A qualitative example from Flux.1-Krea-Dev [15] is provided in Figure 1.

We further interpret the diversity degradation from an entropy perspective (H), where a lower entropy indicates that the generated samples are more predictable and exhibit lower diversity. In particular, longer prompts typically impose more constraints on the generation process, thereby reducing uncertainty and leading to less diverse outputs. For instance, specifying style, camera angle, or composition restricts the feasible region of possible outputs and makes the results more predictable. Formally, let  $\mathbf{X}$  be a random variable representing the sample space for generated samples  $\mathbf{x}$ , and let  $c_s$  and  $c_l$  denote the short and long prompts. Then,

$$H(\mathbf{X} \mid c_l) < H(\mathbf{X} \mid c_s),$$

where the inequality is strict when the additional details in the long prompt provide informative constraints on **X**. The full derivation is provided in Appendix C.1

## 3.3. Prompt Reformulation

Longer prompts typically include more detailed descriptions, thereby constraining the feasible space and reducing output diversity. To mitigate this determinism, we propose to increase the stochasticity of the conditioning process by introducing multiple reformulated prompts during generation. Intuitively, using a set of prompt variants adds "modes" to the conditioning space, relaxing the constraints

<sup>&</sup>lt;sup>1</sup>LPD-Bench is introduced in Section 4.

imposed by a single prompt and expanding the entropy of the resulting latent distribution.

Formally, we define a set of reformulated prompts  $\mathcal{C}_{ref}$ , obtained through transformations from the original prompt c. During inference, the conditional distribution of the sample random variable  $\mathbf{X}$  can be expressed with the reformulated prompts through the law of total probability as a weighted mixture:

$$p(\mathbf{X} \mid c) = \sum_{c' \in C_{\text{ref}}} p(\mathbf{X} \mid c') \, p(c' \mid c). \tag{3}$$

We aim to enhance generation diversity by constructing a valid reformulated prompt set  $C_{ref}$ . The entropy of the resulting distribution can be expressed as (see Appendix C.2):

$$H_n(\mathbf{X} \mid c) = \sum_{c' \in C_{ref}} p(c' \mid c) H(\mathbf{X} \mid c') + I(\mathbf{X}; \mathbf{C}_{ref} \mid c), \quad (4)$$

where  $H_n$  denotes the entropy computed under the cardinality  $|\mathcal{C}_{\mathrm{ref}}| = n$ ,  $\mathbf{C}_{\mathrm{ref}}$  is the random variable representing the reformulated prompt, and  $I(\cdot)$  denotes the conditional mutual information between the generated samples and the reformulated prompts. To ensure that  $\mathcal{C}_{\mathrm{ref}}$  is non-trivial, it is essential that  $H_n$  forms a monotonically increasing sequence with respect to n. In other words, by adding more reformulated prompts, we can progressively enhance the overall generation diversity.

However, the monotonicity of  $H_n$  with respect to n does not generally hold without further assumptions. Under the following conditions: (1) all conditional entropies  $H(\mathbf{X} \mid c')$  are identical (denoted h), (2) each conditional distribution  $p(\mathbf{X} \mid c')$  has disjoint support, and (3) the mixture weights are uniform,  $p(c' \mid c) = 1/n$ , we obtain:

$$H_{n+1} - H_n = \log(n+1) - \log n > 0,$$
 (5)

demonstrating the monotonic increase of entropy with the number of prompt variants. The full proof is provided in Appendix C.3.

**Toy example.** We instantiate the reformulated set by n uniformly weighted 1D Gaussians,  $p_n(x) = \frac{1}{n} \sum_{k=1}^n \mathcal{N}(x; \mu_k, \sigma^2)$ , with identical variance  $\sigma^2$  and means  $\{\mu_k\}$  spaced by  $\Delta = 6\sigma$  to approximate disjoint support, with each component corresponds to a reformulated prompt. The entropy  $H_n$  is estimated numerically via  $-\int p_n(x)\log p_n(x)\,dx$  and compared to the theoretical curve  $h + \log n$ , where  $h = \frac{1}{2}\log(2\pi e\sigma^2)$ . As shown in the bottom of Figure 3, the estimated  $H_n$  increases monotonically with n and closely follows  $h + \log n$ , confirming the analysis. From the top panel, increasing n adds modes and spreads mass across the real line, giving more chances to sample different x values and thus more diverse outcomes; this diversity is also reflected by the Vendi Score (computed from 300 samples per n), which also rises with n.

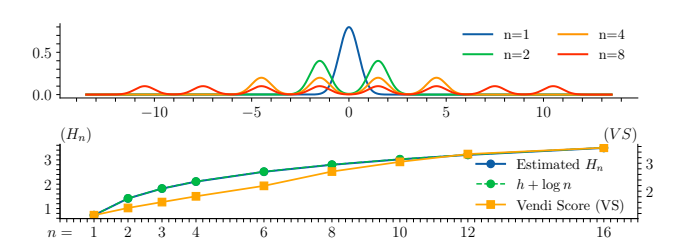


Figure 3. Illustration of the toy example. (Top) 1D Mixture-of-Gaussians for varying n. (Bottom) Estimated entropy  $H_n$  along-side the theoretical curve  $h + \log n$ , together with the Vendi Score.

# 3.4. PromptMoG

Motivated by the toy example, we adopt a simple yet effective sampling strategy based on a MoG formulation, namely PromptMoG. Since the token space is discrete and semantically similar tokens are not positioned closely, we operate directly in the embedding space, where embeddings with similar meanings are naturally organized in close proximity. Formally, the prompt embedding for c is denoted by  $e_c = E(c)$ , where  $E(\cdot)$  is a text encoder. To construct the MoG, we determine how the reformulated prompts should be positioned so that the mixture satisfies the monotonicity assumptions, ensuring that diversity increases as the number of reformulated prompts grows. Once the MoG is defined, we first sample a mode (corresponding to one reformulated prompt) and then perform denoising conditioned on this sampled embedding. Below, we describe how to construct the set of reformulated prompts to meet the required assumptions.

**Identical Entropy.** To ensure that all conditional entropies  $H(\mathbf{X} \mid c_i')$  are similar, we adopt an effective strategy to make each reformulated prompt  $c_i'$  close to the original prompt c. This design offers two advantages: (1) each  $c_i'$  retains similar semantics, resulting in comparable effects on  $\mathbf{x}$  during sampling and thus similar entropy values; and (2) the reformulated prompts stay semantically aligned with the original prompt, preventing unintended deviations in meaning. Since every  $c_i'$  is derived from c, we define a feasible region in the embedding space as:

$$\|\boldsymbol{e}_c - \boldsymbol{e}_{c'_i}\|_2 \le \gamma_{\text{euc}}, \quad \forall i \in \{1, \dots, n\},$$

where  $\gamma_{\rm euc}$  is a predefined similarity threshold controlling the semantic proximity between c and its reformulations. In practice, since  $\gamma_{\rm euc}$  depends on the embedding dimension and is often difficult to determine directly, we first define a cosine similarity measure  $\gamma_{\rm sim}$  and then convert it to the corresponding Euclidean distance:

$$\gamma_{\text{euc}} = \|\boldsymbol{e}_c\|_2 \sqrt{1 - 2\gamma_{\text{sim}}},\tag{6}$$

where we assume that  $\{e_{c'_i}\}$  and  $e_c$  share the same  $\ell_2$  norm.

 $<sup>^2</sup>$ In practice, each Gaussian can be treated as disjoint if the  $\mu_i$  are far apart. A more formal treatment with a truncated version can be used.

Disjointness and Uniform Probability. Defining the feasible region  $\mathcal{C}_{\mathrm{ref}}$  as the Euclidean surface at distance  $\gamma_{\mathrm{euc}}$  from  $e_c$  forms a hypersphere in the embedding space. To ensure uniform mixture probabilities, the reformulated prompt embeddings  $\{e_{c_i'}\}$  are distributed uniformly on this hypersphere such that each embedding is equidistant from the others. This can be achieved using a regular simplex construction, which guarantees maximal and uniform pairwise angular separation:

$$\mathbf{e}_{c_i'}^{\mathsf{T}} \mathbf{e}_{c_i'} = -\gamma_{\mathrm{euc}}^2/(n-1), \quad \forall i \neq j.$$

Since a regular simplex defines a fixed configuration for a given n, a rotation matrix can be applied to generate multiple uniform arrangements on the hyperspherical surface. Further details are provided in Appendix C.4. The reformulated prompts positioned on the hypersphere surface serve as the centers of a Mixture-of-Gaussians (MoG). To maintain disjointness among mixture components, we control the Gaussian variance  $\sigma^2$  such that adjacent distributions remain non-overlapping. In practice,  $\sigma$  is determined relative to the embedding distance  $\gamma_{\rm euc}$ . Specifically, we scale  $\sigma$  proportionally to  $\gamma_{\rm euc}/\sqrt{d}$ , where d is the embedding dimension. This ensures that the component spread adapts to the prompt spacing.

**Overall Generation Pipeline.** The final prompt embeddings are sampled from the constructed MoG, and the subsequent image generation follows the original rectified flow formulation. The complete PromptMoG algorithm and visual illustration are provided in Appendix G.

# 4. LPD-Bench

To systematically study the fidelity and diversity characteristics in long-prompt generation, we introduce LPD-Bench, a benchmark designed to evaluate the generative diversity, semantic fidelity, and aesthetic quality under long and compositionally rich prompts.

# 4.1. Benchmark Design

LPD-Bench includes prompts drawn from diverse categories to ensure broad generalizability. We define a broad set of topics to cover a wide range of visual domains. Specifically, we reference the photography taxonomy in Adobe Lightroom [1] to obtain representative scene categories, and merge semantically similar entries to form 25 distinct topics. Following prior works [13, 23], we employ an LLM to generate detailed long prompts for each topic. Each sample contains a 250–450 word description that spans three aspects: *content, spatial,* and *stylistic* attributes, simulating how humans naturally depict complex scenes. After data cleaning, we retain 1000 high-quality prompts, with 40 per topic. Details of selected topics, gen-

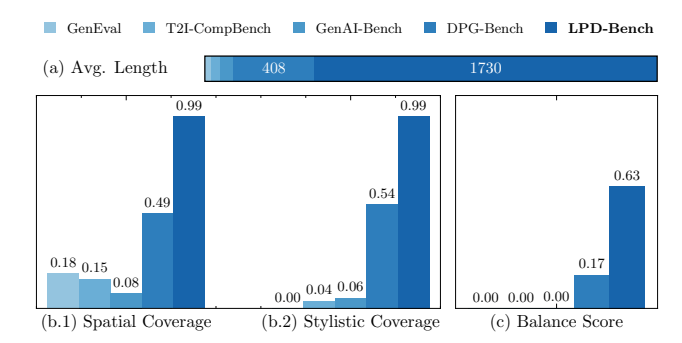


Figure 4. **Comparison of different benchmarks.** For clarity, the average length of the three smallest datasets is ignored.

eration instructions, and data cleaning procedures are provided in Appendix B.

As shown in Figure 4, LPD-Bench provides prompts that are on average  $4\times$  longer than those in existing benchmarks, making it well suited for evaluating long-prompt image generation. In addition, LPD-Bench offers the highest spatial and stylistic coverage, with a substantially larger proportion of prompts including spatial descriptions and stylistic cues that define the visual tone. Prior benchmarks rarely contain long or compositionally rich prompts, and therefore do not capture the complexities inherent in real-world descriptions. By design, most LPD-Bench samples naturally integrate both spatial and stylistic elements, which is reflected in a high *balance score* $^3$ , indicating a more even distribution of these two aspects within each prompt.

#### 4.2. Evaluation Protocol

To evaluate model performance under long and compositionally rich prompts, LPD-Bench adopts a multi-aspect evaluation protocol that assesses generative diversity, semantic fidelity and aesthetic quality.

**Generative Diversity.** We adopt the Vendi Score (VS) [11] to quantify diversity across multiple outputs of the same prompt. Given a set of n generated samples, we first extract visual features using InceptionV3 [31] and DINOv3 [30], and compute all pairwise cosine similarities to form the similarity matrix. A higher VS reflects greater intra-set variability, providing a robust measure of diversity without relying on reference data.

**Semantic Fidelity.** We adopt a **chunk-based** evaluation protocol that assesses fidelity across the *content*, *spatial*, and *stylistic* aspects of each prompt. The long prompt is first segmented into these three components, and then we employ the GPT-4o [14] to generate aspect-specific yes/no questions that capture the essential details of each chunk. For each generated image, we use Owen3-30B [39]

<sup>&</sup>lt;sup>3</sup>Measured as the entropy of the spatial and stylistic tokens within a prompt. Higher indicates a more balanced composition. Please refer to Appendix B.2 for more details.

Table 1. Quantitative results on LPD-Bench. VQA represents the visual question answering score, and AS denotes the aesthetic score. We compute the Vendi Score using both InceptionV3 and DINOv3 as feature extractors. The default image resolution is  $1024 \times 1024$ .

Methods	Content-VQA	Spatial-VQA	Stylistic-VQA	Average			
				VQA	AS	VS-Incep.	VS-DINO
SD3.5-Large [10]	$82.31 \pm 0.28$	$67.91 \pm 0.36$	$78.50 \pm 0.26$	$76.24 \pm 0.20$	$6.83 \pm 0.01$	$2.14 \pm 0.27$	$1.92 \pm 0.43$
+ Chunk	$62.95 \pm 0.37$	$56.43 \pm 0.35$	$69.28 \pm 0.46$	$62.89 \pm 0.26$	$6.69 \pm 0.01$	$2.26 \pm 0.32$	$2.13\pm 0.53$
+ CADS [27]	$70.39 \pm 0.91$	$54.62 \pm 0.55$	$66.05\pm 0.94$	$63.68 \pm 0.50$	$6.26 \pm 0.01$	$2.74 \pm 0.34$	$3.29 \pm 0.72$
+ DiverseFlow [20]	$59.71 \pm 0.50$	$52.45 \pm 0.75$	$45.69 \pm 0.79$	$52.62 \pm 0.41$	$4.14 \pm 0.01$	$2.61 \pm 0.27$	$3.01 \pm 0.64$
+ PromptMoG	$78.66 \pm 0.19$	$65.59 \pm 0.25$	$76.75\pm 0.18$	$73.67 \pm 0.06$	$6.80 \pm 0.01$	$2.20 \pm 0.29$	$2.04 \pm 0.48$
Flux.1-Krea-Dev [15]	$90.51 \pm 0.39$	$75.56 \pm 0.14$	$85.63 \pm 0.23$	$83.90 \pm 0.19$	$7.02 \pm 0.01$	$1.92 \pm 0.26$	$1.71 \pm 0.37$
+ Chunk	$68.28 \pm 0.34$	$62.35 \pm 0.34$	$74.08 \pm 0.29$	$68.24 \pm 0.14$	$6.89 \pm 0.01$	$2.08 \pm 0.34$	$2.12 \pm 0.53$
+ CADS	$87.09 \pm 0.24$	$68.90 \pm 0.44$	$79.57\pm0.55$	$78.52 \pm 0.32$	$6.46 \pm 0.01$	$2.49 \pm 0.28$	$2.57 \pm 0.58$
+ DiverseFlow	$86.29 \pm 0.49$	$72.14 \pm 0.30$	$72.60 \pm 0.25$	$77.01 \pm 0.14$	$5.18 \pm 0.01$	$2.31 \pm 0.27$	$2.13 \pm 0.43$
+ PromptMoG	$88.26 \pm 0.29$	$73.75 \pm 0.20$	$84.82 \pm 0.20$	$82.27\pm 0.12$	$7.02 \pm 0.00$	$2.01 \pm 0.30$	$1.86 \pm 0.43$
CogView4 [41]	$85.84 \pm 0.41$	$74.56 \pm 0.13$	$80.83 \pm 0.20$	$80.41 \pm 0.12$	$6.51 \pm 0.01$	$1.93 \pm 0.27$	$1.50 \pm 0.27$
+ Chunk	$26.32 \pm 0.30$	$35.88 \pm 0.40$	$51.39 \pm 0.41$	$37.87 \pm 0.25$	$5.57\pm 0.01$	$2.31 \pm 0.44$	$2.27\pm 0.75$
+ CADS	$51.08 \pm {\scriptstyle 1.18}$	$48.80 \pm 1.04$	$50.69 \pm 0.56$	$50.19 \pm 0.86$	$4.79\pm 0.03$	$2.99 \pm 0.34$	$3.69 \pm 0.59$
+ DiverseFlow	$81.32 \pm 0.33$	$72.07 \pm 0.33$	$72.84 \pm 0.32$	$75.41 \pm 0.19$	$5.49 \pm 0.01$	$1.97\pm 0.26$	$1.58 \pm 0.32$
+ PromptMoG	$81.18 \pm 0.43$	$70.94 \pm 0.43$	$79.09 \pm 0.39$	$77.07 \pm 0.32$	$6.49 \pm 0.00$	$2.02 \pm 0.31$	$1.63 \pm 0.36$
Qwen-Image [35]	$94.63 \pm 0.14$	$77.81 \pm 0.22$	$87.28 \pm 0.10$	$86.58 \pm 0.07$	$6.64 \pm 0.01$	$1.73 \pm 0.20$	$1.32 \pm 0.17$
+ Chunk	$65.87 \pm 0.36$	$61.85 \pm 0.39$	$76.80 \pm 0.21$	$68.17 \pm 0.16$	$6.66 \pm 0.01$	$1.83 \pm 0.24$	$1.48\pm 0.30$
+ CADS	$84.38 \pm 0.79$	$68.63 \pm 1.00$	$73.42 \pm 0.87$	$75.48 \pm 0.69$	$6.06 \pm 0.03$	$2.74 \pm 0.48$	$2.58 \pm 0.74$
+ DiverseFlow	$82.43\pm 0.32$	$72.41 \pm 0.22$	$58.99 \pm 0.42$	$71.27 \pm 0.18$	$4.80 \pm 0.01$	$2.12 \pm 0.27$	$1.70 \pm 0.40$
+ PromptMoG	$92.31 \pm 0.20$	$75.76 \pm 0.42$	$86.42 \pm 0.19$	$84.83 \pm 0.14$	$6.63 \pm 0.01$	$1.88 \pm 0.25$	$1.49 \pm 0.27$

to answer the chunked questions conditioned on the image, and compute the probability of a "yes" response as the Vision Question Answering (VQA) score [16]. Our chunk-based evaluation reflects not only the overall sentence—image alignment but also whether specific compositional details are faithfully preserved. A higher VQA Score indicates stronger semantic consistency.

**Aesthetic Score** (**AS**). We employ LAION-Aesthetics V2.5 [29, 33] with SigLIP [40] as the backbone to estimate the aesthetic quality of generated images. Higher aesthetic scores indicate a greater human preference and help identify visually pleasing results, while also revealing potential distortions or over-optimized artifacts.

# 5. Experiments

**Setup.** We conduct experiments on **LPD-Bench** using the evaluation metrics introduced in Section 4.2. All experiments are performed on a single NVIDIA H100 GPU with the PyTorch framework. We report the results over **6** random seeds to ensure robustness.

**Baselines.** We compare our method on 4 large-scale T2I models, including SD3.5-Large [10] (8B), Flux.1-Krea-Dev [15] (12B), CogView4 [41] (6B), and Qwen-Image [35] (20B), with CADS [27] and DiverseFlow [20]. We also incorporate *prompt-chunking* baseline to simulate

short prompts, which tend to have higher diversity, as detailed in Appendix E. In addition, we benchmarking autoregressive models, including Janus-Pro-7B [6], NextStep-1 [32], Show-o2 [38], and BLIP3o-NEXT [5] as a reference for our proposed LPD-Bench in Appendix F. All models are evaluated under their default configurations. Details of the hyperparameters are provided in Appendix D.

#### 5.1. Results

Qualitative Comparison. The qualitative results for Flux.1-Krea-Dev, CogView4, and Qwen-Image are shown in Figure 5, and additional comparisons are provided in Appendix H. As illustrated, CADS introduces ill-constrained variations: although diversity increases, semantic fidelity collapses. For instance, the sky disappears and the style becomes distorted in the top example; a checkerboard artifact emerges in the middle example; and incorrect lighting or object placement appears in the bottom example. On the other hand, DiverseFlow suffers from over-optimization, producing visually degraded outputs with incorrect overall styles. In contrast, our constrained sampling generates diverse outputs while preserving the correct semantic content, as reflected by both the Vendi Score and the visual results.

**Quantitative Comparison.** The quantitative results are presented in Table 1. For the chunking baseline, diver-

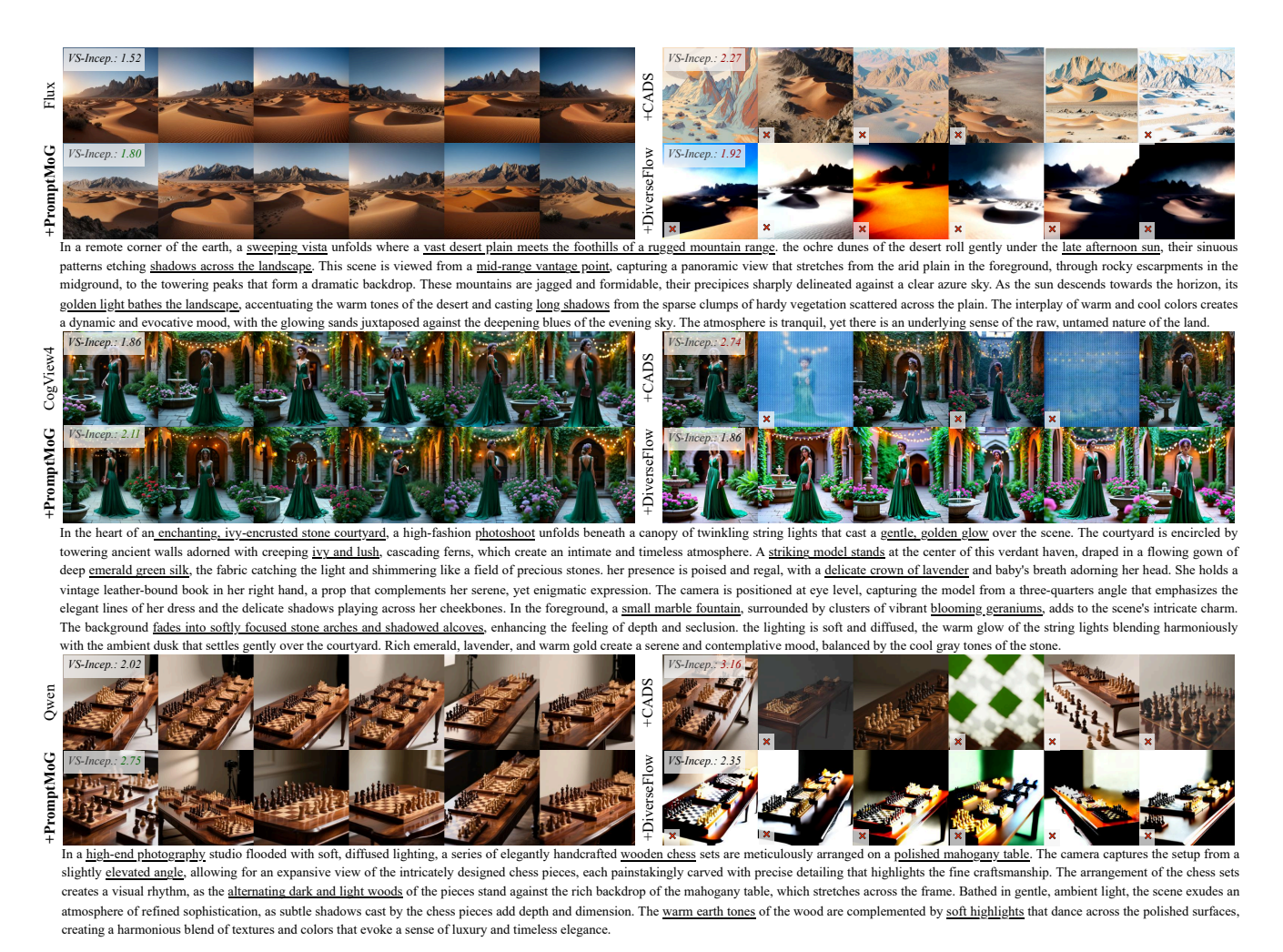


Figure 5. Qualitative comparison with Flux.1-Krea-Dev (top), CogView4 (middle), and Qwen-Image (bottom). Vendi Scores are shown at the top left, and failed outputs are marked at the bottom left. Prompts are truncated with full versions appear in Appendix H.

sity increases, but semantic scores drop noticeably, which is expected since splitting and recombining prompt segments can disrupt the original meaning. CADS similarly introduces severe distortions, consistent with the qualitative findings, as it varies perturbation scales across timesteps without enforcing semantic consistency. DiverseFlow exhibits over-optimization, leading to style degradation that is reflected in both the stylistic VQA and AS metrics. In contrast, our method introduces controlled variability, achieving higher diversity than the original model while consistently preserving semantic integrity and visual quality indicated by VQA and AS.

#### 5.2. Ablation Study

**Settings.** For efficient evaluation, we sample 8 prompts from each theme in LPD-Bench, resulting in a total of **200** prompts for the ablation study. We select Flux.1-Krea-Dev and Qwen-Image as representative models that employ a transformer encoder and a transformer decoder, respec-

tively, to obtain text embeddings. All results are reported as averaged values.

**Effect of**  $\gamma_{\text{sim}}$ .  $\gamma_{\text{sim}}$  defines the feasible region on the high-dimensional sphere. The results of different values are in Figure 6. A higher  $\gamma_{\text{sim}}$  corresponds to a smaller  $\gamma_{\text{euc}}$  as shown in Equation (6), thereby reducing the feasible region. Consequently, reformulated prompts remain closer to the original prompt, leading to higher semantic consistency as reflected by increasing VQA scores. For aesthetics, a smaller sampling space prevents deviation into irrelevant regions, resulting in static or improved aesthetic quality, particularly for Qwen-Image. However, the restricted sampling region limits diversity, yielding lower VS-Incep. and VS-DINO.

**Effect of**  $\sigma$ .  $\sigma$  controls the sampling range of each Gaussian component. The results of different values are in Figure 7. A larger  $\sigma$  expands the sampling space, enhancing diversity as evidenced by higher VS-Incep. and VS-DINO.

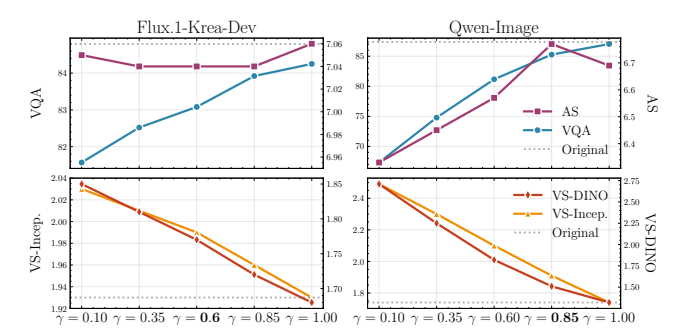


Figure 6. Comparison across different  $\gamma_{sim}$ . The default setting is highlighted in **bold**. Dashed line: w/o. PromptMoG.

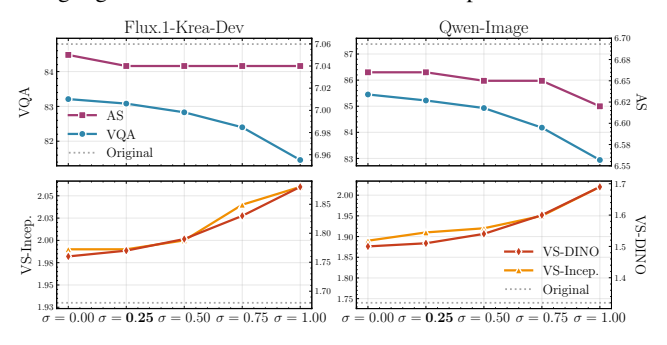


Figure 7. Comparison across different  $\sigma$ . The default setting is highlighted in **bold**. Dashed line: w/o. PromptMoG.

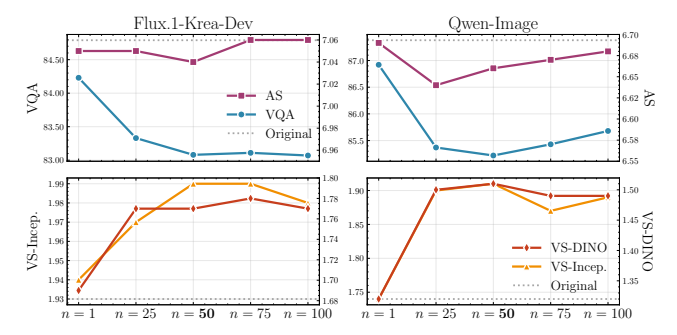


Figure 8. **Comparison across different** *n***.** The default setting is highlighted in **bold**. Dashed line: w/o. PromptMoG.

However, an excessively large  $\sigma$  increases the chance of sampling embeddings that deviate from the semantic center, causing slight semantic drift and lower VQA scores. Since the overall distance to the center remains constrained, the aesthetics score remains nearly stable.

Effect of n. n determines the number of reformulated prompts used to form the MoG. The results of different values are in Figure 8. As predicted by our theoretical analysis, increasing n enhances diversity from n=1 to n=50. When n becomes large (e.g., n=75 or n=100), different Gaussian components begin to overlap, violating the disjointness assumption and removing the guarantee of entropy increase. Notably, variations in n have minimal influence on semantic fidelity and aesthetics, as both are effectively constrained by  $\gamma_{\rm sim}$  and  $\sigma$ .

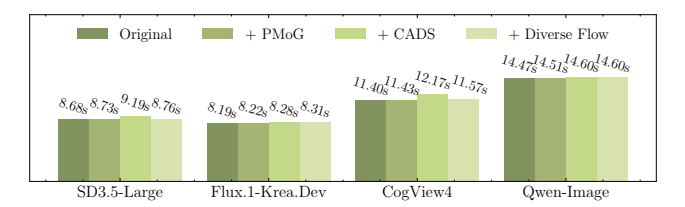


Figure 9. Runtime comparison (s/img) across different approaches. Each result is averaged over 5 runs.

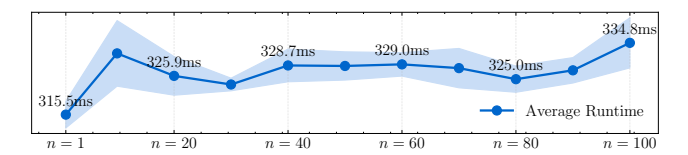


Figure 10. Runtime of PromptMoG under different numbers of modes (n). The shaded area indicates one standard deviation.

# **5.3. Runtime Analysis**

**Between Methods.** We compare the runtime across different approaches, as shown in Figure 9. Each method is executed 5 times, and the average runtime is reported. Overall, different approaches adopt efficient designs. However, our method exhibits a slightly faster trend because prompt embedding sampling is performed only once at the beginning, whereas other approaches require perturbation or optimization at every denoising step.

**Across Modes.** A potential concern is that runtime may increase as the number of reformulated sets (*i.e.*, modes) grows. As illustrated in Figure 10, this is not the case. By vectorizing all operations involved in prompt embedding sampling, our method maintains an almost constant runtime with only a marginal increase as the number of modes grows, demonstrating strong scalability and efficiency.

## **6. Conclusion and Future Work**

In this work, we address the challenge of reduced diversity in long-prompt image generation. With our proposed LPD-Bench, we demonstrate that large-scale SOTA models consistently exhibit a decline in diversity as prompt length increases. To mitigate this issue, we develop a theoretical framework that connects prompt reformulation to entropy and introduce a plug-and-play method, PromptMoG, which samples prompt embeddings from a Mixture-of-Gaussians to enhance diversity while maintaining semantic fidelity. Experiments on four large-scale models, including SD3.5-Large, Flux.1-Krea-Dev, CogView4, and Qwen-Image, validate the effectiveness and generalizability of PromptMoG. For future work, we plan to extend our formulation to other modalities, e.g. images and audio, to enable cross-modal diversification. We also aim to perform space truncation to retain only the most informative subspace, thereby improving semantic preservation with even higher diversity.

## References

- [1] Adobe Inc. 28 types of photography: Styles and genres. https://www.adobe.com/creativecloud/ photography/type.html, 2025. Accessed: 2025-10-31. 2, 5
- [2] Mikołaj Bińkowski, Dougal J. Sutherland, Michael Arbel, and Arthur Gretton. Demystifying MMD GANs. In *International Conference on Learning Representations*, 2018. 2
- [3] Andrew Brock, Jeff Donahue, and Karen Simonyan. Large scale GAN training for high fidelity natural image synthesis. In *International Conference on Learning Representa*tions, 2019. 1
- [4] Qi Cai, Jingwen Chen, Yang Chen, Yehao Li, Fuchen Long, Yingwei Pan, Zhaofan Qiu, Yiheng Zhang, Fengbin Gao, Peihan Xu, et al. Hidream-i1: A high-efficient image generative foundation model with sparse diffusion transformer. arXiv preprint arXiv:2505.22705, 2025. 2
- [5] Jiuhai Chen, Le Xue, Zhiyang Xu, Xichen Pan, Shusheng Yang, Can Qin, An Yan, Honglu Zhou, Zeyuan Chen, Lifu Huang, et al. Blip3o-next: Next frontier of native image generation. *arXiv preprint arXiv:2510.15857*, 2025. 6, 7
- [6] Xiaokang Chen, Zhiyu Wu, Xingchao Liu, Zizheng Pan, Wen Liu, Zhenda Xie, Xingkai Yu, and Chong Ruan. Januspro: Unified multimodal understanding and generation with data and model scaling. arXiv preprint arXiv:2501.17811, 2025. 6, 7
- [7] Gabriele Corso, Yilun Xu, Valentin De Bortoli, Regina Barzilay, and Tommi S. Jaakkola. Particle guidance: noni.i.d. diverse sampling with diffusion models. In *Interna*tional Conference on Learning Representations, 2024. 2, 3
- [8] Mischa Dombrowski, Weitong Zhang, Sarah Cechnicka, Hadrien Reynaud, and Bernhard Kainz. Image generation diversity issues and how to tame them. In *Conference on Com*puter Vision and Pattern Recognition, pages 3029–3039, 2025. 2, 3
- [9] Patrick Esser, Robin Rombach, and Bjorn Ommer. Taming transformers for high-resolution image synthesis. In Conference on Computer Vision and Pattern Recognition, pages 12873–12883, 2021.
- [10] Patrick Esser, Sumith Kulal, Andreas Blattmann, Rahim Entezari, Jonas Müller, Harry Saini, Yam Levi, Dominik Lorenz, Axel Sauer, Frederic Boesel, Dustin Podell, Tim Dockhorn, Zion English, and Robin Rombach. Scaling rectified flow transformers for high-resolution image synthesis. In *International Conference on Machine Learning*, pages 12606–12633, 2024. 2, 6, 8, 12
- [11] Dan Friedman and Adji Bousso Dieng. The vendi score: A diversity evaluation metric for machine learning. *Transactions on Machine Learning Research*, 2023. 2, 5
- [12] Martin Heusel, Hubert Ramsauer, Thomas Unterthiner, Bernhard Nessler, and Sepp Hochreiter. Gans trained by a two time-scale update rule converge to a local nash equilibrium. In *Neural Information Processing Systems*, pages 6629–6640, 2017. 2
- [13] Xiwei Hu, Rui Wang, Yixiao Fang, Bin Fu, Pei Cheng, and Gang Yu. Ella: Equip diffusion models with

- llm for enhanced semantic alignment. arXiv preprint arXiv:2403.05135, 2024. 5
- [14] Aaron Hurst, Adam Lerer, Adam P Goucher, Adam Perelman, Aditya Ramesh, Aidan Clark, AJ Ostrow, Akila Welihinda, Alan Hayes, Alec Radford, et al. Gpt-4o system card. arXiv preprint arXiv:2410.21276, 2024. 5
- [15] Sangwu Lee, Titus Ebbecke, Erwann Millon, Will Beddow, Le Zhuo, Iker García-Ferrero, Liam Esparraguera, Mihai Petrescu, Gian Saß, Gabriel Menezes, and Victor Perez. FLUX.1 Krea [dev]. https://github.com/kreaai/flux-krea, 2025. 2, 3, 6, 7, 8, 15
- [16] Zhiqiu Lin, Deepak Pathak, Baiqi Li, Jiayao Li, Xide Xia, Graham Neubig, Pengchuan Zhang, and Deva Ramanan. Evaluating text-to-visual generation with image-to-text generation. In *European Conference on Computer Vision*, pages 366–384, 2024. 6
- [17] Xingchao Liu, Chengyue Gong, and qiang liu. Flow straight and fast: Learning to generate and transfer data with rectified flow. In *International Conference on Learning Representa*tions, 2023. 3
- [18] Nanye Ma, Mark Goldstein, Michael S Albergo, Nicholas M Boffi, Eric Vanden-Eijnden, and Saining Xie. Sit: Exploring flow and diffusion-based generative models with scalable interpolant transformers. In *European Conference on Computer Vision*, pages 23–40, 2024. 1, 2
- [19] Zichen Miao, Jiang Wang, Ze Wang, Zhengyuan Yang, Lijuan Wang, Qiang Qiu, and Zicheng Liu. Training diffusion models towards diverse image generation with reinforcement learning. In *Conference on Computer Vision and Pattern Recognition*, pages 10844–10853, 2024. 2
- [20] Mashrur M Morshed and Vishnu Boddeti. Diverseflow: Sample-efficient diverse mode coverage in flows. In Conference on Computer Vision and Pattern Recognition, pages 23303–23312, 2025. 2, 3, 6, 8
- [21] Muhammad Ferjad Naeem, Seong Joon Oh, Youngjung Uh, Yunjey Choi, and Jaejun Yoo. Reliable fidelity and diversity metrics for generative models. In *International conference* on machine learning, pages 7176–7185, 2020. 2
- [22] Jonas Oppenlaender. A taxonomy of prompt modifiers for text-to-image generation. *Behaviour & Information Tech*nology, 43(15):3763–3776, 2024. 2
- [23] Dongmin Park, Sebin Kim, Taehong Moon, Minkyu Kim, Kangwook Lee, and Jaewoong Cho. Rare-to-frequent: Unlocking compositional generation power of diffusion models on rare concepts with LLM guidance. In *International Con*ference on Learning Representations, 2025. 5
- [24] William Peebles and Saining Xie. Scalable diffusion models with transformers. In *International Conference on Computer Vision*, pages 4195–4205, 2023. 1, 2, 7
- [25] Dustin Podell, Zion English, Kyle Lacey, Andreas Blattmann, Tim Dockhorn, Jonas Müller, Joe Penna, and Robin Rombach. SDXL: Improving latent diffusion models for high-resolution image synthesis. In *International Con*ference on Learning Representations, 2024. 2
- [26] Robin Rombach, Andreas Blattmann, Dominik Lorenz, Patrick Esser, and Björn Ommer. High-resolution image synthesis with latent diffusion models. In Conference on Com-

- puter Vision and Pattern Recognition, pages 10684–10695, 2022. 1, 2
- [27] Seyedmorteza Sadat, Jakob Buhmann, Derek Bradley, Ot-mar Hilliges, and Romann M. Weber. CADS: Unleashing the diversity of diffusion models through condition-annealed sampling. In *International Conference on Learning Representations*, 2024. 2, 3, 6, 8
- [28] Mehdi SM Sajjadi, Olivier Bachem, Mario Lucic, Olivier Bousquet, and Sylvain Gelly. Assessing generative models via precision and recall. In *Neural Information Processing* Systems, pages 5234–5243, 2018. 2
- [29] Christoph Schuhmann, Romain Beaumont, Richard Vencu, Cade Gordon, Ross Wightman, Mehdi Cherti, Theo Coombes, Aarush Katta, Clayton Mullis, Mitchell Wortsman, Patrick Schramowski, Srivatsa Kundurthy, Katherine Crowson, Ludwig Schmidt, Robert Kaczmarczyk, and Jenia Jitsev. Laion-5b: An open large-scale dataset for training next generation image-text models. In *Neural Information Processing Systems*, pages 25278–25294, 2022. 6
- [30] Oriane Siméoni, Huy V Vo, Maximilian Seitzer, Federico Baldassarre, Maxime Oquab, Cijo Jose, Vasil Khalidov, Marc Szafraniec, Seungeun Yi, Michaël Ramamonjisoa, et al. Dinov3. *arXiv preprint arXiv:2508.10104*, 2025. 5
- [31] Christian Szegedy, Vincent Vanhoucke, Sergey Ioffe, Jon Shlens, and Zbigniew Wojna. Rethinking the inception architecture for computer vision. In *Conference on Computer* Vision and Pattern Recognition, pages 2818–2826, 2016. 5
- [32] NextStep Team, Chunrui Han, Guopeng Li, Jingwei Wu, Quan Sun, Yan Cai, Yuang Peng, Zheng Ge, Deyu Zhou, Haomiao Tang, et al. Nextstep-1: Toward autoregressive image generation with continuous tokens at scale. *arXiv* preprint arXiv:2508.10711, 2025. 6, 7
- [33] Verb. aesthetic-predictor-v2-5. https://github.com/discus0434/aesthetic-predictor-v2-5, 2024.
- [34] Juntong Wang, Huiyu Duan, Jiarui Wang, Ziheng Jia, Guangtao Zhai, and Xiongkuo Min. Tit-score: Evaluating long-prompt based text-to-image alignment via text-toimage-to-text consistency. arXiv preprint arXiv:2510.02987, 2025. 2
- [35] Chenfei Wu, Jiahao Li, Jingren Zhou, Junyang Lin, Kaiyuan Gao, Kun Yan, Sheng-ming Yin, Shuai Bai, Xiao Xu, Yilei Chen, et al. Qwen-image technical report. *arXiv preprint* arXiv:2508.02324, 2025. 2, 6, 7, 8, 21
- [36] Yi-Lun Wu, Hong-Han Shuai, Zhi-Rui Tam, and Hong-Yu Chiu. Gradient normalization for generative adversarial networks. In *International Conference on Computer Vision*, pages 6373–6382, 2021. 1
- [37] Enze Xie, Junsong Chen, Yuyang Zhao, Jincheng YU, Ligeng Zhu, Yujun Lin, Zhekai Zhang, Muyang Li, Junyu Chen, Han Cai, Bingchen Liu, Daquan Zhou, and Song Han. SANA 1.5: Efficient scaling of training-time and inferencetime compute in linear diffusion transformer. In *Interna*tional Conference on Machine Learning, 2025. 1
- [38] Jinheng Xie, Zhenheng Yang, and Mike Zheng Shou. Showo2: Improved native unified multimodal models. In *Neural Information Processing Systems*, 2025. 6, 7

- [39] An Yang, Anfeng Li, Baosong Yang, Beichen Zhang, Binyuan Hui, Bo Zheng, Bowen Yu, Chang Gao, Chengen Huang, Chenxu Lv, et al. Qwen3 technical report. *arXiv* preprint arXiv:2505.09388, 2025. 5
- [40] Xiaohua Zhai, Basil Mustafa, Alexander Kolesnikov, and Lucas Beyer. Sigmoid loss for language image pre-training. In *International Conference on Computer Vision*, pages 11975–11986, 2023. 6
- [41] Wendi Zheng, Jiayan Teng, Zhuoyi Yang, Weihan Wang, Jidong Chen, Xiaotao Gu, Yuxiao Dong, Ming Ding, and Jie Tang. Cogview3: Finer and faster text-to-image generation via relay diffusion. In European Conference on Computer Vision, pages 1–22, 2024. 2, 6, 7, 8, 18
- [42] Le Zhuo, Liangbing Zhao, Sayak Paul, Yue Liao, Renrui Zhang, Yi Xin, Peng Gao, Mohamed Elhoseiny, and Hongsheng Li. From reflection to perfection: Scaling inference-time optimization for text-to-image diffusion models via reflection tuning. In *International Conference on Computer Vision*, pages 15329–15339, 2025. 1

# PromptMoG: Enhancing Diversity in Long-Prompt Image Generation via Prompt Embedding Mixture-of-Gaussian Sampling

# Supplementary Material

# Content

A Reproducibility Statement	2
R LPD-Bench Creation	2
B.1. Data Construction and Filtering	2
B.2 Data Statistics	4
C Proof of Statement	4
C.1. Entropy Comparison for Long and Short Prompts	4
C.2. Entropy with Reformulated Prompt	5
C.3. Monotonic Increasing Property	5
C.4. Regular Simplex	6
D Hyperparameter Setup	6
E Prompt Chunking	7
F. Additional Results with Autoregressive Models	7
G Illustration and Algorithm of PromptMoG	7
H Additional Visualization Comparison	8

# A. Reproducibility Statement

We provide our code in the supplementary materials. To ensure consistent results across different hardware configurations, we generate random noise on the CPU so that runs with the same seed produce *nearly* identical outputs<sup>4</sup>. As a result, both the generated images and the reported scores remain stable across devices. We hope this supports transparent, open-source, and reproducible experimentation.

# **B. LPD-Bench Creation**

# **B.1. Data Construction and Filtering**

We construct LPD-Bench through three stages: (1) deciding the themes, (2) generating a large pool of candidate prompts, and (3) filtering the pool to retain a diverse subset with minimal redundancy. An example of the generated output is shown in Figure 11.

**Prompt Themes.** We adopt the photography taxonomy from Adobe LightRoom [1], which initially defines 28 categories. We consolidate these into 25 representative themes by removing overlapping categories (*e.g.*, merging "Portrait" and "Headshot" into a single category). The final themes are listed in Table 2.

Wildlife Landscape Macro Astrophotography Seascape Real Estate Weather **Botanical** Architecture Urban Aerial **Portrait** Fashion **Sports** Candid Event Food Product Still Life Automotive Fine Art Black and White Abstract Surreal Long Exposure

Table 2. Categories of LPD-Bench.

**Pool Generation.** Our system and instruction prompts, following recommended practice from [22], are shown in the colored boxes below to generate an initial pool of **60** samples for each topic. Each sample includes a long prompt together with its corresponding chunked descriptions and yes/no questions across the *semantic*, *spatial*, and *stylistic* aspects.

**Prompt Filtering.** To reduce redundancy and ensure diversity, we perform pairwise similarity-based filtering to select a subset of **40** prompts that are maximally distinct for each theme. Formally, let  $C = \{c_i\}_{i=1}^N$  denote the complete set of generated prompts, where each prompt  $c_i$  contains three descriptive components: semantic, spatial, and stylistic. We embed each component using a pretrained sentence encoder  $f_{\theta}(\cdot)$  to obtain:

$$\mathbf{s}_i = f_{\theta}(c_i^{\text{semantic}}), \quad \mathbf{r}_i = f_{\theta}(c_i^{\text{spatial}}), \quad \mathbf{t}_i = f_{\theta}(c_i^{\text{stylistic}}).$$

The final representation of a prompt is the concatenation of the normalized embeddings:

$$\mathbf{e}_i = \operatorname{concat} \left[ \operatorname{norm}(\mathbf{s}_i), \operatorname{norm}(\mathbf{r}_i), \operatorname{norm}(\mathbf{t}_i) \right] \in \mathbb{R}^{(3 \times d)}.$$

We then compute the cosine similarity matrix  $S_{ij}$  and the average similarity  $\bar{s}_i$  for each prompt:

$$S_{ij} = \frac{\mathbf{e}_i^{\top} \mathbf{e}_j}{\|\mathbf{e}_i\|_2 \|\mathbf{e}_j\|_2}, \quad \bar{s}_i = \frac{1}{N-1} \sum_{j \neq i} S_{ij}.$$

A smaller  $\bar{s}_i$  indicates that a prompt is less correlated with others. Therefore, we select the final subset  $C_{\text{sel}}$  consisting of K=100 prompts corresponding to the lowest  $\bar{s}_i$  values:

$$C_{\text{sel}} = \{ c_i \mid i \in \operatorname{argsort}(\bar{s})_{1 \cdot K} \}.$$

<sup>&</sup>lt;sup>4</sup>GPU operations may be non-deterministic, but the impact on results is negligible.

#### System Prompt for Long Prompt Generation

You are an expert visual prompt engineer and researcher specializing in generating long, compositionally rich prompts for text-to-image tasks.

## **Instruction Prompt for Long Prompt Generation**

#### Your task is to:

- 1. Write a long, detailed, and coherent text-to-image prompt based on the given theme
- 2. Ensure the prompt is not similar to any of the existing prompts
- 3. Decompose the scene into **semantic**, **spatial**, and **stylistic** aspects
- 4. For each aspect, provide **chunked descriptions** and **diverse QA pairs** for evaluation

#### 1. Theme

Theme: {theme}

Description: {description}

Existing prompts: {existing\_prompts}

#### 2. Prompt Creation Rules

Overall Structure & Length

- Target length: 250-450 words
- Format: Coherent narrative paragraph(s), NOT keyword lists
- Tone: Third-person, present-tense, cinematic description
- Coherence: Maintain internal consistency throughout

## Required Components

Your prompt MUST include these six elements in natural language:

- (1) Subject Terms: Main subject(s) and their characteristics, environment and setting details, subject relationships and activities.
- (2) Composition & Spatial Arrangement: Camera perspective, framing, depth (foreground, midground, background), scale relationships.
- (3) Lighting & Atmosphere: Light source, light quality, atmospheric conditions, shadows and highlights.
- (4) Color Palette & Mood: Dominant colors, color relationships, color temperature, emotional tone.
- (5) Style Modifiers: Artistic style, medium characteristics, technical approach.
- (6) Quality Boosters: Technical excellence markers, professional indicators, recognition markers.

#### 3. Description and QA Generation Rules

For each aspect—semantic, spatial, and stylistic:

Description Chunks: Provide 2–4 short declarative statements (10–25 words each). Each chunk describes ONE observable visual fact.

Yes/No Questions: Provide 2–4 questions per aspect. All correct answers must be "Yes". Questions must be unambiguous, verifiable, aspect-aligned, affirmative, and specific.

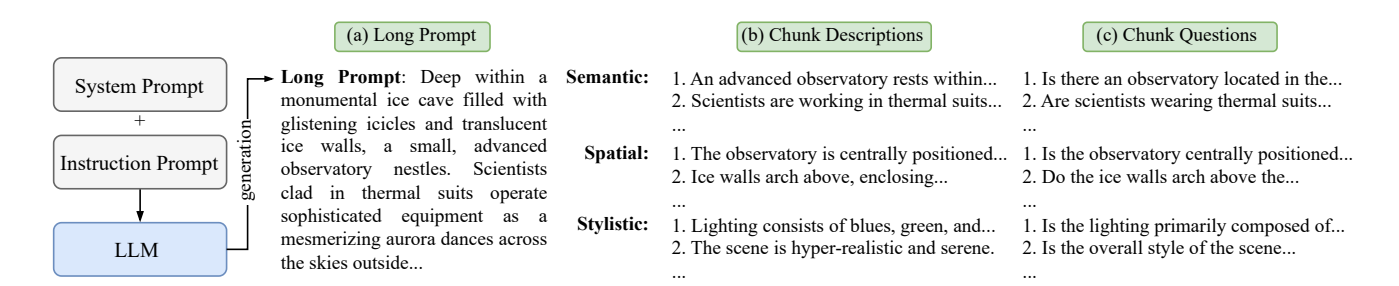


Figure 11. **Example of a generated long-prompt.** Each sample includes a long prompt along with chunk-level descriptions and yes/no questions (answers are always yes) covering the *semantic*, *spatial*, and *stylistic* aspects for evaluation.

## **B.2. Data Statistics**

To analyze the linguistic composition of the benchmark datasets, we compute several statistics based on part-of-speech and phrase-level analyses. For each prompt c, we first process its text using a pretrained spaCy<sup>5</sup> model to obtain a tokenized sequence  $\{w_i\}_{i=1}^{N_c}$ , excluding punctuation and stop words. Each token or phrase is then categorized into one of two aspects, spatial or stylistic, as illustrated in Figure 4. Multi-word phrases are detected using spaCy's PhraseMatcher with predefined spatial and stylistic phrase lists generated by GPT-40, while single tokens are tagged according to their membership in the corresponding lexical sets.

Let  $n_{\rm spa}(c)$  and  $n_{\rm sty}(c)$  denote the number of spatial and stylistic tokens (or phrase spans) identified in prompt c. We define their normalized densities as:

$$d_{\rm spa}(c) = \frac{n_{\rm spa}(c)}{N_c}, \qquad d_{\rm sty}(c) = \frac{n_{\rm sty}(c)}{N_c}, \label{eq:dspa}$$

where  $N_c$  is the total number of valid tokens in the prompt.

A prompt is considered to *cover* an aspect if it satisfies either a minimum density or a minimum count criterion:

$$\mathrm{cover}_{\mathrm{spa}}(c) = \mathbf{1}_{\left\{\mathrm{d}_{\mathrm{spa}}(c) \geq \tau_{\mathrm{spa}} \ \vee \ \mathrm{n}_{\mathrm{spa}}(c) \geq k_{\mathrm{spa}}\right\}},$$

where  $\mathbf{1}_{\{\cdot\}}$  is the indicator function and analogously for the stylistic category. We set  $\tau_{\rm spa} = \tau_{\rm sty} = 0.05$  and  $k_{\rm spa} = k_{\rm sty} = 5$  in all experiments. The overall dataset-level *spatial* and *stylistic coverage* are computed as the proportions of prompts that satisfy each condition.

To quantify the balance between the two aspects within a prompt, we compute a normalized entropy score:

$$H(c) = -\sum_{a \in \{\text{spa,sty}\}} \tilde{d}_a(c) \, \log \tilde{d}_a(c),$$

where  $\tilde{d}_a(c) = d_a(c)/(d_{\rm spa}(c) + d_{\rm sty}(c))$ . The balance index  $H(c) \in [0,1]$  equals 1 when spatial and stylistic terms are evenly distributed and approaches 0 when dominated by a single category. We report the dataset-level average  $\bar{H} = \frac{1}{|C|} \sum_{c \in C} H(c)$  as the *balance score*. Additionally, we measure the *average prompt length* using the number of characters.

## C. Proof of Statement

## C.1. Entropy Comparison for Long and Short Prompts

Let X be a random variable representing generated samples, and let  $c_s$  and  $c_l$  denote the short prompt and the long prompt, respectively. Assume that the long prompt contains all the information of the short prompt plus additional details u, i.e.:

$$c_l = (c_s, u).$$

We show that the conditional entropy under the long prompt is no larger than that under the short prompt:

$$H(\mathbf{X} \mid c_l) \le H(\mathbf{X} \mid c_s). \tag{7}$$

*Proof.* By the definition of conditional mutual information, we have:

$$I(\mathbf{X}; u \mid c_s) = H(\mathbf{X} \mid c_s) - H(\mathbf{X} \mid c_s, u). \tag{8}$$

After rearranging, we have:

$$H(\mathbf{X} \mid c_s, u) = H(\mathbf{X} \mid c_s) - I(\mathbf{X}; u \mid c_s). \tag{9}$$

Since mutual information is always nonnegative,  $I(\mathbf{X}; u \mid c_s) \geq 0$ , it follows that:

$$H(\mathbf{X} \mid c_l) = H(\mathbf{X} \mid c_s, u) \le H(\mathbf{X} \mid c_s). \tag{10}$$

Therefore, conditioning on a longer (more informative) prompt can only reduce or leave unchanged the uncertainty in X.  $\Box$ 

<sup>5</sup>https://github.com/explosion/spaCy

# C.2. Entropy with Reformulated Prompt

Let  $\mathbf{X}$  be a random variable representing the generated samples, and let c and c' denote the target prompt and a reformulated prompt, respectively. We define  $\mathbf{C}_{\text{ref}}$  as the random variable corresponding to the set of possible reformulated prompts  $\mathcal{C}_{\text{ref}}$ , whose distribution is given by  $p(c' \mid c)$ . That is,  $\mathbf{C}_{\text{ref}}$  models the stochastic process of drawing a reformulated prompt c' conditioned on the target prompt c. Additionally,  $I(\mathbf{X}; \mathbf{C}_{\text{ref}} \mid c)$  is the conditional mutual information between the generated sample and the reformulated prompt given the original prompt c.

We show that the conditional entropy under the target prompt can be expressed as a weighted combination of the conditional entropies under the reformulated prompts:

$$H_n(\mathbf{X} \mid c) = \sum_{c' \in \mathcal{C}_{ref}} p(c' \mid c) H(\mathbf{X} \mid c') + I(\mathbf{X}; \mathbf{C}_{ref} \mid c), \tag{11}$$

where  $H_n$  denotes the entropy computed when the cardinality  $|\mathcal{C}_{\text{ref}}| = n$ .

*Proof.* From the chain rule of conditional entropy, we have

$$H(\mathbf{X}, \mathbf{C}_{ref} \mid c) = H(\mathbf{X} \mid \mathbf{C}_{ref}, c) + H(\mathbf{C}_{ref} \mid c) = H(\mathbf{C}_{ref} \mid \mathbf{X}, c) + H(\mathbf{X} \mid c). \tag{12}$$

Rearranging the last two expressions yields

$$H(\mathbf{X} \mid c) = H(\mathbf{X} \mid \mathbf{C}_{ref}, c) + H(\mathbf{C}_{ref} \mid c) - H(\mathbf{C}_{ref} \mid \mathbf{X}, c). \tag{13}$$

Recognizing that the last two terms form the conditional mutual information, we obtain

$$H(\mathbf{X} \mid c) = H(\mathbf{X} \mid \mathbf{C}_{ref}, c) + I(\mathbf{X}; \mathbf{C}_{ref} \mid c), \quad \text{with} \quad I(\mathbf{X}; \mathbf{C}_{ref} \mid c) = H(\mathbf{C}_{ref} \mid c) - H(\mathbf{C}_{ref} \mid \mathbf{X}, c). \tag{14}$$

Finally, by expanding  $H(\mathbf{X} \mid \mathbf{C}_{ref}, c)$  over the discrete set  $\mathcal{C}_{ref}$ , we have

$$H(\mathbf{X} \mid c) = \underbrace{\sum_{c' \in \mathcal{C}_{ref}} p(c' \mid c) H(\mathbf{X} \mid c')}_{H(\mathbf{X} \mid \mathbf{C}_{ref}, c)} + I(\mathbf{X}; \mathbf{C}_{ref} \mid c), \tag{15}$$

which completes the proof.

#### C.3. Monotonic Increasing Property

Let X be a random variable representing the generated samples x, and let c and c' denote the target prompt and a reformulated prompt from a set  $\mathcal{C}_{\text{ref}}^{(n)} \triangleq \{c'_1, \cdots, c'_n\}$ , respectively.

## **Assumptions:**

- (A1) (Equal component entropies)  $H(\mathbf{X} \mid c_i') = h$  for all i.
- (A2) (Disjoint supports) The conditional densities  $p(\mathbf{X} \mid c_i')$  have pairwise disjoint supports  $S_i$ , i.e.,  $S_i \cap S_j = \emptyset$  for  $i \neq j$ .
- (A3) (Uniform weights)  $p(c'_i \mid c) = 1/n$  for all i.

With the assumptions above, we have the monotonic increasing property:

$$H_{n+1}(\mathbf{X} \mid c) - H_n(\mathbf{X} \mid c) = \log(n+1) - \log(n) > 0.$$
 (16)

*Proof.* By (A3), for any  $\mathbf{x} \in S_i$  we have  $p(\mathbf{X} \mid c) = \frac{1}{n}p(\mathbf{X} \mid c_i')$ , and  $p(\mathbf{X} \mid c_j') = 0$  for  $j \neq i$ . Therefore:

$$H_n(\mathbf{X} \mid c) = -\int p(\mathbf{X} \mid c) \log p(\mathbf{X} \mid c) d\mathbf{x}$$
(17)

$$\stackrel{\text{By (A2)}}{=} -\sum_{i=1}^{n} \int_{S_i} \frac{1}{n} p(\mathbf{X} \mid c_i') \log \left( \frac{1}{n} p(\mathbf{X} \mid c_i') \right) d\mathbf{x}$$
(18)

$$= -\frac{1}{n} \sum_{i=1}^{n} \int_{S_i} p(\mathbf{X} \mid c_i') \log p(\mathbf{X} \mid c_i') d\mathbf{x} + \frac{1}{n} \sum_{i=1}^{n} \int_{S_i} p(\mathbf{X} \mid c_i') \log n d\mathbf{x}$$
 (19)

$$= \frac{1}{n} \sum_{i=1}^{n} H(\mathbf{X} \mid c_i') + \log n.$$
 (20)

By (A1),  $\frac{1}{n} \sum_{i=1}^{n} H(\mathbf{X} \mid c_i') = h$ , hence  $H_n(\mathbf{X} \mid c) = h + \log n$ . The stated difference  $H_{n+1} - H_n = \log(n+1) - \log n > 0$  follows immediately, proving strict monotonicity.

# C.4. Regular Simplex

Given a base embedding  $e_c \in \mathbb{R}^d$ , a radius  $\gamma > 0$ , and a target number of variants  $n \geq 2$ , construct centers  $\{\mu_i\}_{i=1}^n \subset \mathbb{R}^d$  such that:

$$\|\mu_i - \mathbf{e}_0\|_2 = \gamma$$
 and  $\mu_i^{\top} \mu_i = -\gamma^2/(n-1) \ (i \neq j),$  (21)

i.e., all points lie on the hypersphere of radius  $\gamma$  around  $e_c$  and are maximally/equally separated.

**Constraint:** Let  $\{e_{c'_i}\}_{i=1}^n$  satisfy:

$$\|\mathbf{e}_{c_i'}\|_2 = 1, \quad \mathbf{e}_{c_i'}^{\top} \mathbf{e}_{c_j'} = \begin{cases} 1, & i = j, \\ -\frac{1}{n-1}, & i \neq j. \end{cases}$$
 (22)

These are the vertices of a regular simplex on the unit sphere  $S^{n-2}$ . They achieve equal pairwise angles  $\arccos\left(-\frac{1}{n-1}\right)$  and equal pairwise distances.

Let  $I_n$  be the  $n \times n$  identity and  $\mathbf{1}_n$  the all-ones vector. Define the  $n \times n$  centering matrix  $H = I_n - \frac{1}{n} \mathbf{1}_n \mathbf{1}_n^{\top}$  and set:

$$V = H \in \mathbb{R}^{n \times n}$$
.

Let the thin SVD be  $V = U\Sigma W^{\top}$  and take the first n-1 right singular vectors  $W_{1:(n-1)}$ . Then the n rows of

$$\tilde{U} = W_{1:(n-1)} \in \mathbb{R}^{n \times (n-1)}$$

form a centered, orthonormal configuration. Normalize each row to unit norm to obtain  $\mathbf{u}_1, \dots, \mathbf{u}_n$  with the simplex inner products above. For any  $d \geq n-1$ , pad each  $\mathbf{u}_i$  with zeros to  $\hat{\mathbf{u}}_i \in \mathbb{R}^d$ , apply an arbitrary orthogonal transform  $R \in \mathrm{O}(d)$  (e.g., a rotation matrix), and set:

$$\mathbf{e}_{c'} = \mathbf{e}_c + \gamma R \hat{\mathbf{u}}_i \quad \text{for } i = 1, \dots, n.$$
 (23)

Then  $\|\boldsymbol{e}_{c_i'} - \boldsymbol{e}_c\|_2 = \gamma$  and  $\boldsymbol{e}_{c_i'}^{\top} \boldsymbol{c}_{c_j'} = -\gamma^2/(n-1)$  for  $i \neq j$ .

# D. Hyperparameter Setup

We summarize the hyperparameters used in our experiments in Table 3. For CogView4 and Qwen-Image, which employ a transformer decoder to obtain text embeddings, we use a larger  $\gamma$ . Unlike encoder-based models, decoder-based embeddings lack strong semantic locality, and an overly small  $\gamma$  can lead to unstable or degraded outputs. This effect is evident in Section 5.2.

Table 3. Hyperparameter settings for different models.

Model	$\gamma$	$\sigma$	n	Inference Step
SD3.5-Large [24]	0.7	0.25	50	28
Flux.1-Krea-Dev [15]	0.6	0.25	50	28
CogView4 [41]	0.95	0.2	50	28
Qwen-Image [35]	0.85	0.25	50	28

# E. Prompt Chunking

We adopt prompt chunking based on our earlier observation that generation diversity decreases as prompt length increases. To address this, we split each prompt into several overlapping chunks and average their embeddings. This strategy effectively simulates using shorter textual segments to represent a long prompt. Formally, given a prompt c consisting of k sentences  $[c_{s_1}, c_{s_2}, \cdots, c_{s_k}]$ , we define a window size k with a stride of one to group sentences, forming k-k overlapping chunks. We then compute the final embedding k by averaging the embeddings of all chunks:

$$\boldsymbol{e}_{\boldsymbol{c}'} = \frac{1}{k - w} \sum_{i=1}^{k - w} E(\hat{c}_i), \quad \text{with} \quad \hat{c}_i \triangleq [c_{s_i}, \cdots, c_{s_{i + w}}], \tag{24}$$

where E denotes a text encoder.

# F. Additional Results with Autoregressive Models

To complement our benchmark for evaluating long-prompt fidelity and diversity, we additionally assess several state-of-theart autoregressive (AR) models, as reported in Table 4. Compared with RF-based models, AR models consistently exhibit higher diversity. We attribute this to their inference strategy: once the initial noise is sampled, RF-based models follow a fixed denoising trajectory and cannot introduce new stochasticity. In contrast, AR models resample pixels (or tokens) sequentially, giving each position multiple opportunities to adopt different values. This sequential resampling inherently encourages diverse outputs. These observations further underscore the importance of developing plug-and-play methods that enhance the diversity of RF-based models without sacrificing semantic fidelity.

Table 4. Additional results of autogressive-based generation models on LPD-Bench. VQA represents the visual question answering score, and AS denotes the aesthetic score. We compute the Vendi Score using both InceptionV3 and DINOv3 as feature extractors. The default image resolution is  $1024 \times 1024$ , while methods marked with a superscript indicate their supported resolution.

Methods	Content-VQA	Spatial-VQA	Stylistic-VQA	Average			
				VQA	AS	VS-Incep.	VS-DINO
Janus-Pro-7B <sup>384</sup> [6]	$79.23 \pm 0.59$	$67.82 \pm 0.17$	$79.87 \pm 0.28$	$75.64 \pm 0.27$	$5.59 \pm 0.01$	$2.27 \pm 0.26$	$2.11 \pm 0.42$
NextStep-1 <sup>512</sup> [32]	$88.35\pm0.26$	$74.81\pm0.22$	$83.34 \pm 0.27$	$82.17 \pm 0.15$	$6.01 \pm 0.05$	$2.05\pm 0.28$	$1.88 \pm 0.40$
Show-o2 [38] BLIP3o-NEXT [5]	$86.16 \pm 0.49 \\ 85.39 \pm 0.20$	$75.03 \pm 0.33 \\ 73.74 \pm 0.23$	$82.00 \pm 0.17 \\ 81.99 \pm 0.21$	$81.06 \pm 0.26 \\ 80.37 \pm 0.11$	$6.05 \pm 0.01 \\ 6.41 \pm 0.01$	$\begin{array}{c} 1.90 \pm 0.20 \\ 1.92 \pm 0.23 \end{array}$	$\begin{array}{c} 1.56 \pm 0.26 \\ 1.59 \pm 0.28 \end{array}$

## G. Illustration and Algorithm of PromptMoG

We provide a visualization of the feasible region in Figure 12. Given a distance threshold  $\gamma$ , the set of embeddings forms a spherical surface, shown in blue. Applying the regular simplex approach distributes n reformulated embeddings uniformly on this sphere shown in red, maximizing their pairwise separation. These embeddings serve as the centers of the Gaussian components, forming a Mixture-of-Gaussians (MoG) used in the final sampling process.

In Algorithm 1, we present the complete algorithm of our approach. The only additional step required during inference is sampling a prompt embedding from the constructed MoG. Once sampled, this embedding is reused throughout the generation process, which follows the original rectified flow formulation without modification.

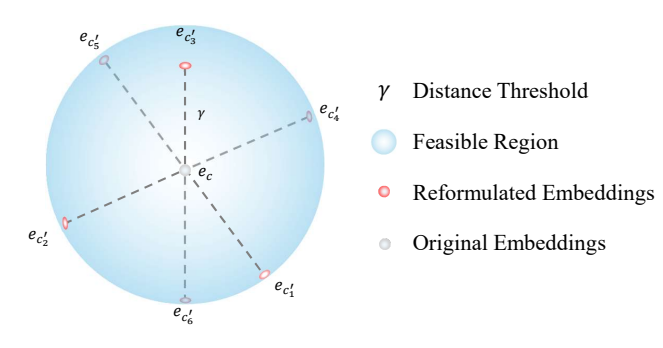


Figure 12. Illustration of the feasible region for n=6 in a 3D embedding space.

# Algorithm 1: Generation with PromptMoG

```
Input: prompt c; text encoder E(\cdot); distance threshold \gamma_{\mathrm{euc}}; noise scale \sigma; number of modes n; model \mathbf{v}_{\theta}(\cdot); total timesteps t_{\mathrm{max}} Output: Generated image \mathbf{x}_{0}

1 \mathbf{e}_{c} \leftarrow E(c) // Embedding from original prompt 2 \{\mathbf{u}_{i}\}_{i=1}^{n} \leftarrow vertices of a simplex on the d-sphere 3 \mathbf{e}_{i} \leftarrow \mathbf{e}_{c} + \gamma_{\mathrm{euc}} \mathbf{u}_{i}, \quad i=1,\ldots,n 4 \mathbf{e}_{c'} \sim \frac{1}{n} \sum_{i} \mathcal{N}(\mathbf{e}_{i}, \sigma^{2}\mathbf{I}) // Sampled from MoG 5 \mathbf{x}_{t_{\mathrm{max}}} \sim \mathcal{N}(\mathbf{0}, \mathbf{I}) 6 for k = max, \ldots, 1 do // Denoising \mathbf{x}_{t_{k}} 7 \mid \mathbf{x}_{t_{k-1}} \leftarrow \mathbf{x}_{t_{k}} + (t_{k-1} - t_{k}) \mathbf{v}_{\theta}(\mathbf{x}_{t_{k}}, t_{k}, \mathbf{e}_{c'}) 8 end
```

# H. Additional Visualization Comparison

Detailed versions of each prompt in Figure 5 can be found in Figure 13.

We provide additional qualitative comparisons between PromptMoG (ours), CADS [27], and DiverseFlow [20] on SD3.5-Large [10] (Figure 14), Flux.1-Krea-Dev [15] (Figure 15), CogView4 [41] (Figure 16), and Qwen-Image [35] (Figure 17). For each model, we include 3 comparisons across different themes. Consistent with Figure 5, CADS frequently produces checkerboard artifacts or deviates significantly from the prompt. DiverseFlow often yields over-optimized outputs with distorted or unappealing styles; although it performs slightly better on CogView4, oversaturated colors remain evident. Overall, our method consistently generates diverse outputs while preserving alignment with the original prompt.

9 return  $x_0$ 

(Flux - Landscape) In a remote corner of the earth, a sweeping vista unfolds where a vast desert plain meets the foothills of a rugged mountain range. The ochre dunes of the desert roll gently under the late afternoon sun, their sinuous patterns etching shadows across the landscape. This scene is viewed from a mid-range vantage point, capturing a panoramic view that stretches from the arid plain in the foreground, through rocky escarpments in the midground, to the towering peaks that form a dramatic backdrop. These mountains are jagged and formidable, their precipices sharply delineated against a clear azure sky. As the sun descends towards the horizon, its golden light bathes the landscape, accentuating the warm tones of the desert and casting long shadows from the sparse clumps of hardy vegetation scattered across the plain. The interplay of warm and cool colors creates a dynamic and evocative mood, with the glowing sands juxtaposed against the deepening blues of the evening sky. The atmosphere is tranquil, yet there is an underlying sense of the raw, untamed nature of the land. This landscape is rendered in ultra-high resolution, capturing the fine details of the rocky terrain, the delicate ripples in the sand, and the sharp edges of the peaks, embodying a masterful application of landscape photography techniques.

(CogView4 - Fashion) In the heart of an enchanting, ivy-encrusted stone courtyard, a high-fashion photoshoot unfolds beneath a canopy of twinkling string lights that cast a gentle, golden glow over the scene. The courtyard is encircled by towering ancient walls adorned with creeping ivy and lush, cascading ferns, which create an intimate and timeless atmosphere. A striking model stands at the center of this verdant haven, draped in a flowing gown of deep emerald green silk, the fabric catching the light and shimmering like a field of precious stones. Her presence is poised and regal, with a delicate crown of lavender and baby's breath adorning her head. She holds a vintage leather-bound book in her right hand, a prop that complements her serene, yet enigmatic expression. The camera is positioned at eye level, capturing the model from a three-quarters angle that emphasizes the elegant lines of her dress and the delicate shadows playing across her cheekbones. In the foreground, a small marble fountain, surrounded by clusters of vibrant, blooming geraniums, adds to the scene's intricate charm. The background fades into softly focused stone arches and shadowed alcoves, enhancing the feeling of depth and seclusion. The lighting is soft and diffused, the warm glow of the string lights blending harmoniously with the ambient dusk that settles gently over the courtyard. rich emerald, lavender, and warm gold create a serene and contemplative mood, balanced by the cool gray tones of the stone. This visual narrative is captured with exquisite detail and clarity, evoking a sense of refined elegance and whimsical mystery, akin to the timeless artistry of fine art portraiture. Every element, from the model's elegant pose to the play of light on the ivy-leafed walls, is rendered in sharp focus, presenting a harmonious blend of natural beauty and haute couture in an image of professional excellence.

(Qwen - Product) In a high-end photography studio flooded with soft, diffused lighting, a series of elegantly handcrafted wooden chess sets is meticulously arranged on a polished mahogany table. The camera captures the setup from a slightly elevated angle, allowing for an expansive view of the intricately designed chess pieces, each painstakingly carved with precise detailing that highlights the fine craftsmanship. The arrangement of the chess sets creates a visual rhythm, as the alternating dark and light woods of the pieces stand against the rich backdrop of the mahogany table, which stretches across the frame. Bathed in gentle, ambient light, the scene exudes an atmosphere of refined sophistication, as subtle shadows cast by the chess pieces add depth and dimension. The warm earth tones of the wood are complemented by soft highlights that dance across the polished surfaces, creating a harmonious blend of textures and colors that evoke a sense of luxury and timeless elegance. The choice of a minimalistic setting enhances the focus on the chess sets, allowing their exquisite details to dominate the composition in visual clarity. Captured with high-definition clarity and artistic finesse, the image portrays a perfect balance between light and shadow, form and function, encapsulating both artistic and commercial appeal. The photograph's overall style embodies the essence of classic product photography, where each element is perfectly aligned to create a cohesive narrative that speaks of tradition, quality, and excellence in design.

Figure 13. Illustration of the full prompts used in Figure 5. Themes are indicated at the beginning of each prompt in bold.



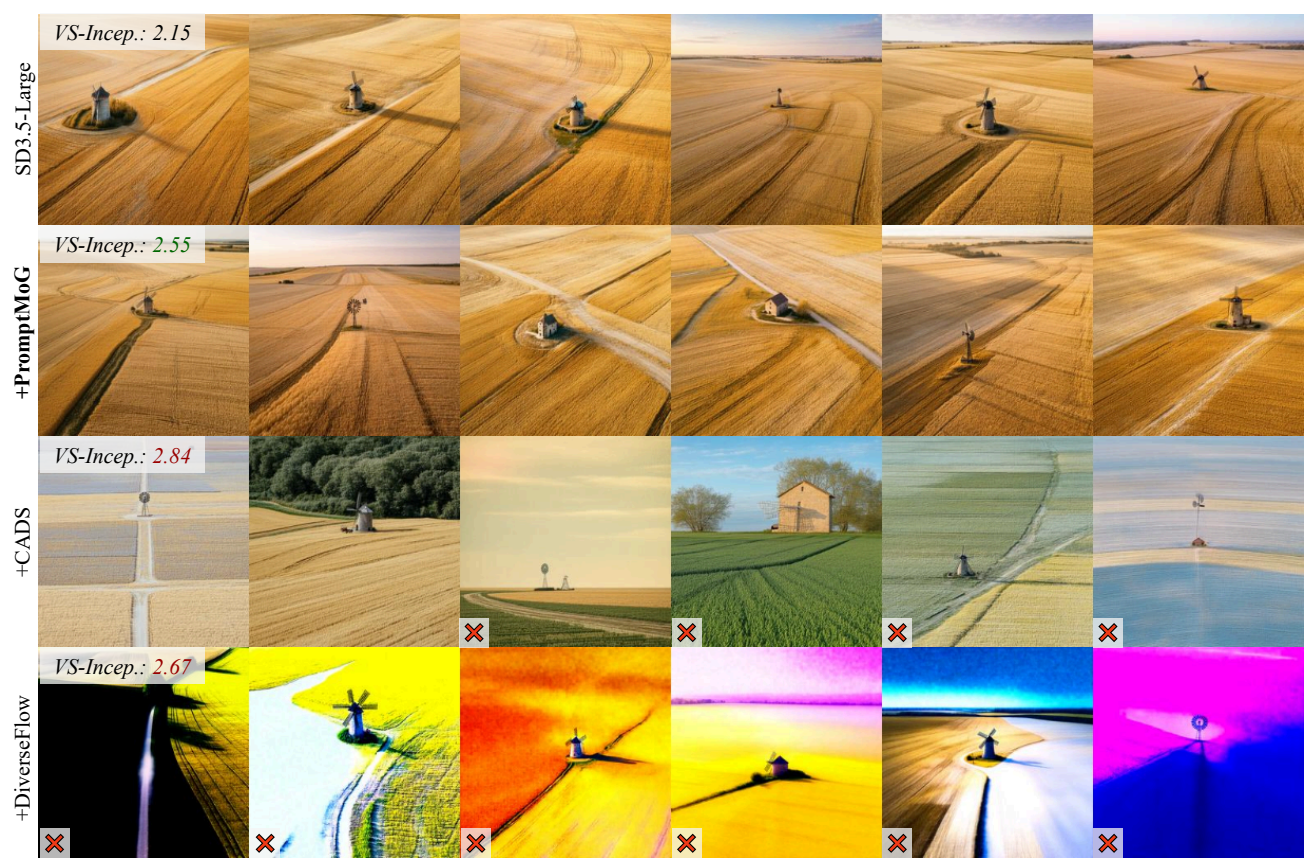
In a quiet, secluded grove at the edge of a sprawling countryside estate, an elaborate renaissance-style manor emerges majestically from a veil of mist, its grandeur enhanced by the meticulous design and artistry of its intricate stone facade. The manor, with its expansive wings and central courtyard, stands as a testament to architectural elegance and historic opulence, its stone walls adorned with carved reliefs depicting scenes from classical mythology. The scene is captured from a slightly elevated perspective, offering a comprehensive view of the manor's symmetry and the formal gardens that stretch elegantly from its base. In the foreground, neatly arranged boxwood hedges and meticulously aligned gravel pathways guide the viewer's eye towards the manor, while the midground is dominated by the graceful rise of the manor itself. Beyond, the background is a rolling tapestry of green fields and distant wooded hills, merging subtly into the horizon under a soft, overcast sky. The manor is bathed in the diffused light of an overcast morning, softening the shadows and lending an air of serene timelessness to the scene. This gentle illumination enhances the muted tones of the stonework, interplaying with the soft greens of the gardens and the subdued grays of the sky, creating a mood of tranquil elegance and understated luxury. The architectural style is captured in a classic fine art photography approach, emphasizing the depth and texture of the stone, the symmetry of the design, and the gentle allure of the surrounding landscape. The final image is rendered in high resolution, with crisp detail ensuring the intricate carvings and the texture of the stone are vividly portrayed, underscoring the sense of timeless beauty and masterful craftsmanship inherent in the architecture.

(a) Theme: Architecture



Nestled amidst a <u>lush urban landscape</u>, a newly constructed modern villa captures the attention with its striking design and positioning. This architectural masterpiece is thoughtfully situated on a generous corner plot, surrounded by meticulously <u>manicured gardens and towering palm trees</u> that sway gently in the breeze. The villa's façade showcases an <u>elegant blend of glass, steel, and natural stone</u>, exuding a sense of contemporary sophistication while harmoniously integrating with the verdant surroundings. From a <u>slightly elevated angle</u>, one can appreciate the villa's expansive layout, featuring a spacious outdoor terrace that seamlessly connects to an <u>infinity pool</u>, offering breathtaking views of the skyline beyond. The foreground is framed by a <u>cobblestone driveway leading to</u> a sleek, double-height entrance, where floor-to-ceiling windows allow sunlight to flood the interior spaces. As the sun begins to set, the villa is bathed in warm, golden hues that accentuate the textures of the stone and provide a dramatic contrast against the deepening blues of the dusk sky. This cinematic lighting creates a cozy yet luxurious atmosphere, enhanced by the soft glow of strategically placed outdoor lighting along the pathways and garden beds. The color palette embraces <u>earthy tones and muted greens</u>, complementing the villa's natural stone elements and lush garden backdrop. Inside, the villa features an <u>open-plan design</u> characterized by minimalist elegance and a <u>seamless flow between indoor and outdoor</u> living spaces. Innovative lighting design highlights architectural features and artwork, while large glass doors slide away to incorporate the terrace and garden into the living area. Captured in high-resolution, with a keen eye for detail and composition, this real estate photograph conveys both the luxury and liveability of the property, inviting potential buyers to envision their future in this exquisite home.

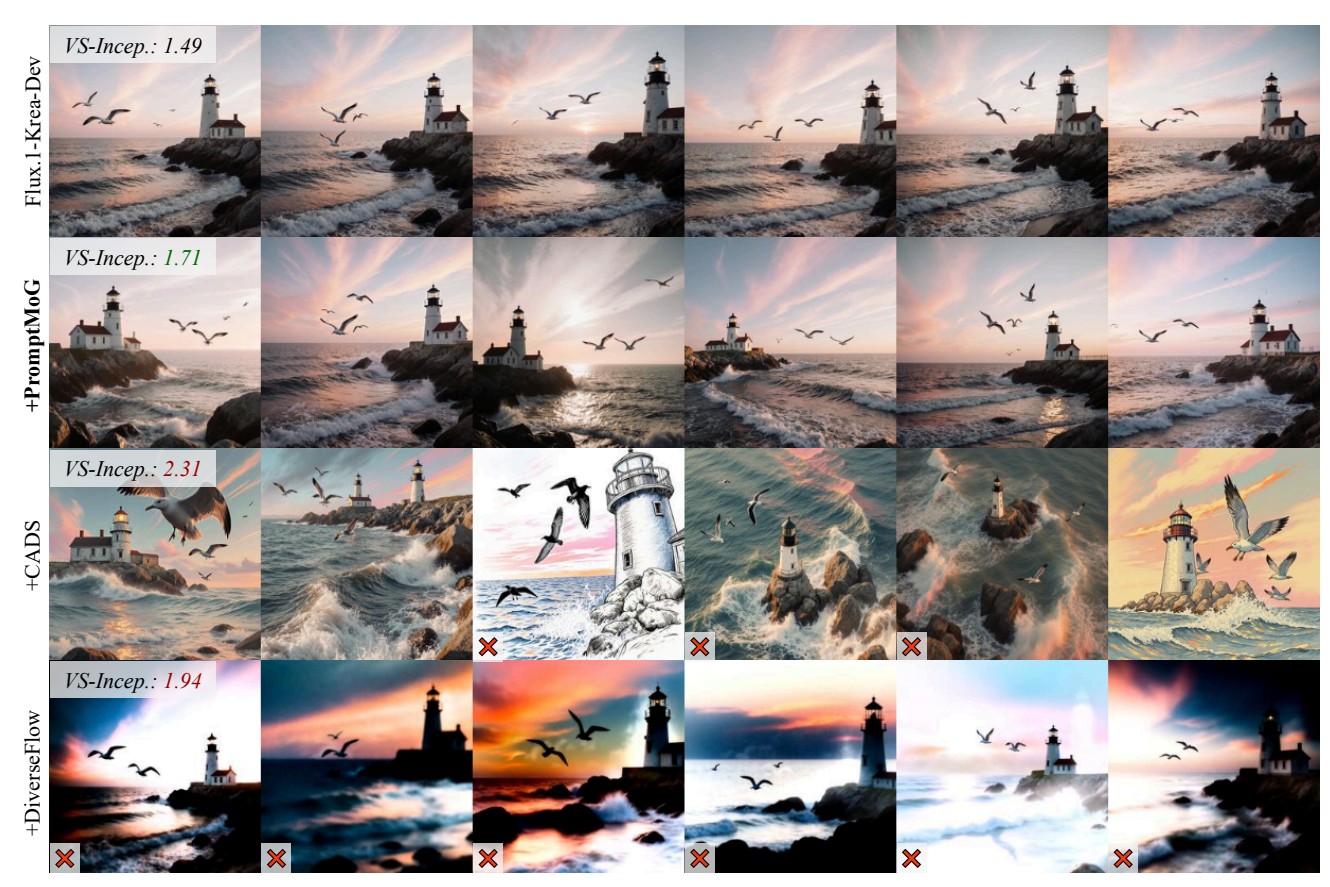
(b) Theme: Real Estate



From the lofty vantage of a circling drone, a sprawling golden wheat field spreads in rhythmic undulations, stretching to meet the distant horizon where azure sky kisses the earth. At the heart of this expansive tableau stands a solitary, ancient windmill, its robust structure weathered by countless seasons yet standing resilient against the whispering breeze. The drone captures this scene with a slight tilt towards the northwest, placing the windmill modestly off-center, allowing the vastness of the field to dominate the frame. Feathered lines of tractor trails carve deliberate patterns into the crops, guiding the gaze inwards towards the historic edifice. As the sun sets, the light dances softly across the landscape, casting the windmill's elongated shadow as a diagonal streak across the golden sea. The soft hues of dusk, a harmonious blend of gentle pinks and purples, overlay the scene, suggesting tranquility and nostalgia. The colors shift subtly from the cool lavender of the distant sky to the warm amber tones that caress the rippling waves of wheat, promoting a serene and reflective mood. The style echoes the poetic realism of landscape photography, capturing the textures of the field and the windmill with meticulous detail and clarity, achieved through state-of-the-art drone technology, the image exudes professional precision, revealing every grain of wheat as well as the crumbling masonry of the windmill. Such a composition promises a breathtaking view that is both masterful in technique and evocative in emotion, destined to linger in the viewer's memory long after the scene fades from view.

(c) Theme: Aerial

Figure 14. **Qualitative comparison with SD3.5-Large [10].** Vendi Scores are shown at the top left, and failed outputs are marked at the bottom left. Themes are indicated in each sub-caption.



In the tranquil embrace of <u>dawn</u>, a vast expanse of <u>shimmering ocean</u> stretches across the horizon, its surface a dance of glistening <u>ripples under the caress of a gentle breeze</u>. The scene unfolds before a solitary weathered lighthouse perched on a rocky promontory, its steadfast silhouette standing resolute against the early morning sky. A pair of <u>seagulls</u> glide gracefully over the waters, their wings slicing through the crisp air as they ride the thermals that rise from the warming sea. The lighthouse, a sentinel of the coast, stands at the scene's fulcrum, its base rooted amidst boulders that jut defiantly into the sea. The camera captures the scene from a <u>low vantage point at the water's edge</u>, slightly skewed to the right, framing the lighthouse on one side while allowing the ocean to recede into the distant horizon on the other, enhancing the vastness of the seascape. In the fore, gentle waves foam and break against the rocky shoreline, adding a dynamic rhythm that contrasts the scene backdrop. As the new day unfurls, the sky is awash with pastel hues, where soft pinks mix with the cool blues of dawn, intersected by warm streaks of orange, capturing the onset of sunlight peeking above the far horizon. This interplay of colors bathes the scene in a soothing, ethereal ambiance, evoking a sense of calm and contemplation. <u>Seabirds wheel above</u> in the soft light, their reflections casting elongated shadows upon the rippling water. The photograph is meticulously composed in the style of fine art seascape photography, emphasizing the intricacies of light and texture across the scene. Each detail is captured with stunning clarity and precision, a testament to masterful technique and an eye for oceanic grandeur, resulting in an image that is both professional and award-winning in its execution.

(a) Theme: Seascape



In the untouched wilderness of the <u>arctic tundra</u>, an awe-inspiring sight unfolds as a majestic polar bear explores its icy domain. The <u>bear, with its thick, lustrous white fur</u>, stands <u>at the edge of a jagged glacier</u>, peering into the crystalline depths of an ice-choked fjord below. The camera captures this magnificent creature from a <u>low vantage point</u>, emphasizing its imposing stature against the endless expanse of ice and sky. framed to highlight the bear's grandeur, the composition places the animal on the lower left quadrant, surrounded by the stark beauty of its environment. in the foreground, <u>ice floes drift languidly on the water's</u> surface, while in the <u>background</u>, the towering cliffs of an ancient glacier rise majestically, their blue and white hues echoing the frigid palette of the scene. Bathed in the ethereal glow of the arctic sun, which hangs low in the sky, the landscape is suffused with a haunting mix of <u>soft blues and shimmering whites</u>, casting long, delicate shadows across the ice. The scene captures the serene, yet unforgiving nature of this remote region, as the gentle lapping of the waves against the ice brings a peaceful yet eerie soundtrack. The high-definition clarity of the photograph reveals exquisite details, from the bear's textured fur to the intricate patterns on the ice, rendered with professional precision and a documentary photojournalism aesthetic, reminiscent of award-winning wildlife photography. This image captures not just a moment, but the essence of an entire ecosystem, fragile and majestic in its raw, untouched beauty.

(b) Theme: Wildlife



In the remote reaches of a tranquil highland plateau, a lone stargazer is nestled comfortably into the soft grass, her gaze fixed firmly upon the sprawling night sky above. She is surrounded by a suite of high-tech observing equipment laid out in precise order, each piece strategically positioned to capture the celestial canvas. The setting is a grassy meadow bordered by shadowy forests, where the land unfolds into gentle undulations leading toward the distant horizon. Overhead, the heavens are alive with a brilliant constellation spread, as galaxies and nebulae blink into crystalline clarity. The symphony of the universe is rendered in meticulous detail, viewed from a low angle that envelops the scene in a wide perspective. The celestial objects form an expansive backdrop, while the immediate foreground hosts the observer and her equipment, creating a layered composition. Soft moonlight bathes the landscape, casting delicate highlights over the stargazer's silhouette and her instruments, while the darkness of the sky is punctuated by the faint glow of the milky way, creating an ethereal ambiance. The atmosphere is clear and crisp, with a gentle breeze stirring the surrounding grasses. The color palette of the night sky is a mesmerizing gradient of deep indigo and silvery whites, offset by the warm golden hue of the telescope's metallic finish, lending the scene an aura of contemplative wonder. The style is reminiscent of illustrative surrealism, capturing the essence of both solitude and cosmic discovery with a dreamlike quality. The image is executed with professional precision, boasting high resolution and sharpness that captures every star's glint and every grassy blade's swaying motion, emphasizing both technical excellence and artistic mastery.

(c) Theme: Astrophotography

Figure 15. **Qualitative comparison with Flux.1-Krea-Dev [15].** Vendi Scores are shown at the top left, and failed outputs are marked at the bottom left. Themes are indicated in each sub-caption.



In a secluded corner of a <u>sun-drenched courtyard</u>, an <u>elderly couple</u> stands poised before an exquisitely weathered stone wall, <u>adorned with climbing ivy</u> that casts intricate patterns of shadow and light. The couple, wearing <u>finely tailored outfits</u> that exude timeless elegance, <u>holds hands</u> with a gentle, enduring intimacy. The camera captures them <u>at eye level</u>, allowing the viewer to connect with the warmth in their expressions and the subtle grace in their stance. positioned <u>slightly off-center</u>, they allow room for the surrounding environment's texture to enrich the composition. The courtyard <u>stretches out behind them</u>, leading the eye along a path bordered by meticulously tended flowerbeds filled with vibrant blooms. <u>Soft afternoon sunlight</u> filters through the high branches of nearby trees, creating dapples of light that dance across the scene, highlighting the couple's delicate features and the subtle wrinkles that tell stories of shared years. The light imbues the space with a gentle, <u>atmospheric warmth</u>, bouncing off the couple's faces with a flattering, golden hue. A palette of warm earth tones and floral pastels dominates the visual, with soft amber and pale pinks creating a serene, nostalgic ambiance. Captured in the style of classical portrait photography, the scene evokes the elegance of a bygone era while maintaining a certain contemporary freshness. The image is rendered in exquisite detail, allowing each leaf, petal, and texture of the stone to be almost palpable, resonating with the viewer on an emotional level. This masterful composition, reminiscent of award-winning photography, combines excellent resolution and clarity to create a lasting impression.

(a) Theme: Portrait



In the <u>shadow of towering rocky cliffs and under a sweeping cerulean sky</u>, an exhilarating rock climbing competition is in full swing. The scene unfolds on an <u>expansive natural wall</u>, where climbers are scattered across the rugged surface like determined specks against a vast canvas of ochre and sandstone. The camera captures the scene from a <u>dynamic low angle</u>, accentuating the sheer verticality and imposing nature of the cliff face. At center stage, a young climber, clad in a vivid red harness and chalk-covered hands, reaches up towards a narrow ledge, muscles taut with effort and concentration etched on her face. Below her, ropes snake across the ground, managed by a focused belayer who stands in the foreground, providing a sense of scale to the daunting ascent. Sunlight <u>spills over the scene from the left</u>, casting sharp contrasts and highlighting the <u>intricate textures of the rock</u>, each crevice and outcrop sharply defined. Despite the bright daylight, the atmosphere is charged with the quiet intensity of concentration and the occasional encouraging shout from the gathered crowd, whose muted hues of attire blend naturally with the earthy tones of the scene. The color palette is <u>dominated by warm</u>, <u>sunlit browns and reds of the rock face</u>, punctuated by the vibrant gear of the climbers. This moment captures the raw spirit of adventure and the primal challenge of man vs. nature, a testament to human endurance and skill. The resulting image possesses a documentary realism, with high-resolution clarity that celebrates the meticulous details of both the environment and the climbers in action, akin to an award-winning photo that tells its own epic tale.

(b) Theme: Sport



In a <u>bustling urban coffee shop</u>, the <u>morning sun streams through tall glass windows</u>, casting long shadows across textured wooden floors. The central figure, a young woman dressed in casual attire, is deeply engrossed in writing on a laptop, surrounded by the comforting chaos of her surroundings. Her face, framed by loose curls, <u>is softly lit by the screen's glow</u>, contrasting with the vibrant movements around her. <u>To her right</u>, a <u>barista with a focused expression</u> skilfully crafts a latte, steam swirling above the espresso machine. Nearby, a group of friends animatedly share stories, their laughter punctuating the ambient hum of the café. The scene captures an intricate tapestry of urban life, where individual moments unfold within a larger, interconnected narrative. The camera adopts a <u>slightly elevated angle</u>, offering a panoramic view of the space, with the woman writer <u>subtly off-center to highlight her quiet concentration</u> amidst the dynamic backdrop. In the background, the <u>open kitchen reveals brief glimpses</u> of bustling activity, chefs in motion as they prepare fresh pastries. The atmosphere is lively yet intimate, suffused with the rich aroma of coffee and freshly baked bread. Natural light interacts with warm interior lighting, creating a cozy and inviting mood. A palette of muted browns, soft greens, and subtle terracotta hues envelops the scene, evoking a sense of warmth and camaraderie. This candid moment, captured with the precision of a seasoned photojournalist, exudes a documentary-style realism, rich in detail and texture, with a crisp 8k resolution enhancing the clarity and vibrancy of each element within the frame.

(c) Theme: Candid

Figure 16. **Qualitative comparison with CogView4 [41].** Vendi Scores are shown at the top left, and failed outputs are marked at the bottom left. Themes are indicated in each sub-caption.



The grand ballroom of the opulent victorian mansion is abuzz with celebration as the wedding reception unfolds in full swing. Guests clad in elegant attire mingle gracefully, their laughter blending with the soft strings of a live chamber orchestra. The intricate parquet floor gleams under the glow of a majestic chandelier that hangs from the ornately plastered ceiling, scattering light like droplets of starlight across the room. At the heart of the ballroom stands a sumptuous banquet table, adorned with a lavish spread of culinary delights and towering floral arrangements in hues of ivory and blush. In the background, the newlyweds share a tender dance, their silhouettes twirling in harmony against the gilded walls that speak of timeless elegance. Captured from an elevated angle, the scene showcases the grandeur of the venue, with the camera drawing the viewer's eye from the intricate details of the floral centerpieces in the foreground to the elegantly arched windows draped with rich velvet curtains in the background. Evening light pours through the windows, mingling with the soft amber glow of the chandelier, creating an ethereal ambiance that wraps the guests in a warm embrace. The color palette of deep burgundy, gold, and cream evokes a sense of romance and splendor, while the understated elegance of the decor marries traditional grandeur with contemporary grace. Shot in a fine art style, the photograph combines meticulous composition and lighting, capturing the essence of celebration and intimacy in an award-winning, high-resolution image that balances sharpness and depth with artistic flair, inviting viewers to immerse themselves in the joyful occasion.

(a) Theme: Event



In the dimly lit recess of a vintage greenhouse, a meticulously arranged still life emerges, featuring an eclectic assortment of botanical specimens and antique gardening tools. A large, glass-topped wooden table serves as the central stage, upon which an old, weathered watering can sits, its surface speckled with patches of rust, embodying the passage of time. A collection of terracotta pots in varying sizes encircles the can, each brimming with an assortment of succulents and ferns that spill over the rims in a cascade of lush greenery. Nestled amongst the plants is an ornate, cast-iron birdcage, its intricate patterns casting delicate shadows onto the table. The composition is viewed in three-quarter perspective, creating an inviting sense of depth that invites the viewer to step closer, revealing more details with each new angle. The foreboding green shadows cast by the glass ceiling above instill the scene with a subtle, mysterious atmosphere, softened by the muted afternoon sun diffused through dusty panes. light filters through, dappling the scene with a gentle play of soft highlights and shadowy undertones. The color palette is a harmonious blend of earthy browns and vibrant greens, with occasional flecks of rust-red and the muted pastels of flowering succulents. This gentle, organic color scheme evokes a feeling of tranquility and quiet introspection, reinforced by the softened light. The photograph exudes a vintage artistic style, reminiscent of 19th-century botanical illustrations, enhanced by the subtle grain of film photography, capturing every detail with sharp precision. The resulting image is a testament to professional craftsmanship, where every leaf and artifact is rendered in breathtaking clarity, exuding an award-winning level of detail and composition.

(b) Theme: Still Life



Nestled within the timeless charm of an abandoned industrial complex, a meticulously crafted metal sculpture of a bird, wrought from iron and steel, stands poised and alone. The sculpture, with its wings slightly unfurled, evokes a sense of dynamic motion frozen in time. This intricate artwork is placed near a rusted conveyor belt, with a backdrop of tall, arched windows that cast a mosaic of shadows across cracked concrete floors. The composition captures the scene from a mid-level angle, framing the sculpture slightly off-center to the right, allowing the vast scale of the windows and decaying architecture to dominate the left side of the image. The windows are covered in a fine layer of dust, filtering the pale morning light to create a soft, diffused glow that highlights the texture of the corroded metal and the feathers' detailed etchings. The absence of color shifts focus to the interplay of light and shadow, where the dark rivets and welds contrast with the lighter surfaces. Despite the stark monochromatic palette, the scene exudes a nostalgic yet melancholic atmosphere, reminiscent of a bygone era when the factory thrived with life and activity. The style echoes the precision and emotive depth found in classic black and white fine art photography, focusing on form and contrast. The high-resolution image captures every aspect of the scene with crystal-clear sharpness, from the finest dust motes suspended in the air to the intricacies of the sculpture, offering a professional-grade visual experience that feels both intimate and expansive.

(c) Theme: Black and White

Figure 17. **Qualitative comparison with Qwen-Image [35].** Vendi Scores are shown at the top left, and failed outputs are marked at the bottom left. Themes are indicated in each sub-caption.